## *Quasi-elastic Neutron Transfer at the Barrier* [B]

W. Reisdorf[1], J.V. Kratz.[2], R. Bellwied[2], W. Brüchle[1], H. Keller[2], K. Lützenkirchen[2], M. Schädel[1], K. Sümmerer[1], G. Wirth[1]
[1] GSI Darmstadt, [2] Institut für Kernchemie, Universität Mainz

Mass and charge distributions for binary reaction channels have been measured for the reactions of $^{86}$Kr with $^{76}$Ge, $^{104}$Ru, and $^{130}$Te at the Coulomb barrier using chemical separations and γ-ray spectroscopy [1]. These systems span the region where dynamical hindrance to complete fusion sets in. The binary reactions were subdivided into two components associated with i) reflection from the outer barrier (quasielastic), and ii) reseparation after passing the barrier (complex reactions). The sum of cross sections for complex reactions and evaporation residues from complete fusion was reproduced by a barrier passing calculation. It was conduded [1] that the fusion probability is limited primarily by reseparation after passing the barrier , and that the reseparation occurs predominantly in the early phase before the unconditional saddlepoint is reached.

Concerning the quasielastic, and in particular the one-nucleon transfer channels, we found cross sections that were very different in the three systems, and, within the same system, for pickup relative to stripping reactions, despite similar $Q_{gg}$ values , in contrast to the smooth systematics of *van den Berg et al.* [2,3] 25 % above the barrier. Following Ref. 2, we have plotted in Fig. 1 the six 'reduced' one-neutron cross sections $\sigma_{1n}\,(B_i\,B_f)^{1.1}$ obtained in our work versus the respective $Q_{gg}$ values. Here, $B_i$ and $B_f$ are the neutron separation energies in the initial and final channels. Also shown for reference is the smooth curve obtained in Ref. 3 by a fit to a large number of such reduced cross sections for above-the-barrier reactions. The order-of-magnitude scatter of our data is particularly striking.

In order to explore further this intriguing observation we have compiled one-neutron transfer data from the literature, limited to a narrow energy window ($0.97 \leq E_{cm} / V_{Bass} \leq 1.06$) around the barrier. The resulting compilation is shown in Fig. 2. The symbols distinguish whether the light partner nucleus was the donor or the acceptor. Obviously, the very large scatter of the points which is in striking contrast to the smooth systematics at higher energies [3], does not correlate with this distinction. As for fusion reactions, we are witnessing here also for one-nucleon transfer reactions an increased complexity in measured cross sections right at or below the barrier. One must conclude that the energy dependence of one-neutron transfer cross sections in going from the barrier energy to 25 % above it must be very different for the various systems and cannot be understood in terms of Q-values alone.

The data suggest that quasi-elastic nucleon transfer channels are influenced by the 'adjacent' complex reaction channels: For $^{86}$Kr + $^{130}$Te, for example, we find a reduced one-neutron pickup cross section that is about three times larger than the stripping cross section. Likewise, the one-proton stripping reaction is about nine times more abundant than the proton-pickup reaction, and $\sigma_{+2n}$ is larger than $\sigma_{-1n}$. Generally, the cross sections are large when the corresponding isotope is close to the maximum of the underlying complex-reaction channels and small when the direction of the transfer is opposite to the collective trend of the complex reactions. We suggest that the coupling to the collective trend of the complex reactions creates a polarization field that favors matching even for strongly negative Q-values.

1. W. Reisdorf et al., Z. Phys. A, in press
2. A.M. van den Berg et al., Phys. Rev. Lett. 56, 572 (1986)
3. K.E. Rehm et al., Phys. Rev. C42, 2497 (1990)

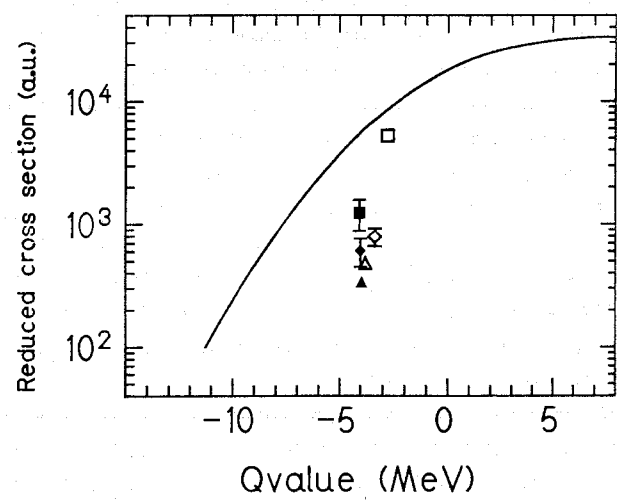


Fig. 1: Measured one-neutron transfer-cross sections as a function of the corresponding $Q_{gg}$ values. Squares: $^{130}$Te target; diamonds: $^{104}$Ru target; triangels: $^{76}$Ge target. Closed (open) symbols refer to stripping (pickup). The smooth curve is from refs. [2,3].

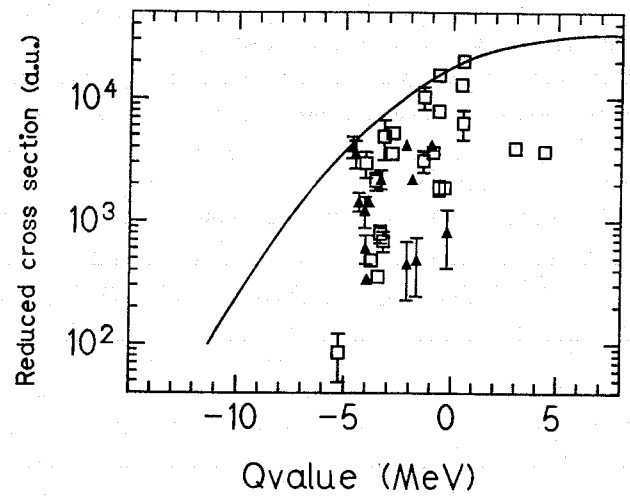


Fig. 2: Systematics of one-neutron transfer-cross sections close to the Coulomb barrier energy. Pickup by the lighter partner: open squares, stripping of the lighter partner: closed triangels.

# Inclusive Measurements of Electromagnetic Dissociation Cross Sections

Th. Aumann [1)], W. Brüchle [2)], J.C. Hill [3)], J.V. Kratz [1)]
M. Schädel [2)], E. Stiel [1)], K. Sümmerer [2)], G. Wirth [2)]
[1)]Institut für Kernchemie, Universität Mainz, [2)]GSI, Darmstadt
[3)]Iowa State University, Ames, Iowa 50011, USA

Electromagnetic excitation of giant resonances by relativistic heavy ions and their subsequent decay by neutron evaporation ("Electromagnetic Dissociation", ED) has first been studied at the BEVALAC [1] with projectiles up to $^{139}$La and energies between 1.26 GeV/u and 2.1 GeV/u. While good agreement between experimental data and a simple Weizsäcker-Williams (WW) calculation is observed for medium-Z nuclei, the extrapolation of experimental data to higher projectile charges leads to much lower cross sections than calculated. The availability of relativistic heavy-ion beams from SIS has made it possible to perform an experimental study of ED also for very heavy systems. We have measured cross sections for the one-neutron removal from $^{197}$Au targets by 1.7 GeV/u $^{20}$Ne and 1 GeV/u $^{86}$Kr, $^{197}$Au and $^{209}$Bi projectiles.

Cross sections were determined by measuring off-line the residual activity in the bombarded targets with calibrated Ge-detectors. Production of $^{196}$Au from secondary reactions in the target was determined by bombarding simultaneously three targets with different thicknesses and extrapolating to zero target thickness. The beam particles hitting the targets were counted with two plastic scintillators, except for the Ne beam, where the beam intensity was monitored with a calibrated secondary-electron transmission monitor [2]. The nuclear contribution to the one-neutron-removal cross section was calculated with the internuclear-cascade model ISABEL [3] and is about 40% for the $^{197}$Au($^{20}$Ne,X)$^{196}$Au reaction and 5% for the $^{197}$Au($^{209}$Bi,X)$^{196}$Au reaction.

The resulting ED cross sections for the 1n-out channel are shown in Fig.1 together with the BEVALAC data [1] and a WW calculation including single-phonon electric dipole and electric quadrupole excitations. In Fig.2 all experimental cross sections are scaled to the same bombarding energy of 1 GeV/u using the energy dependence of the ED process as calculated with the WW procedure. Our data agree very well with that observed by Hill et al.[1] and the new points for Au and Bi beams confirm the trend that the electromagnetic part of the 1n-out cross sections for very heavy ions is systematically overestimated by the WW theory. The measured ED cross section for the $^{197}$Au($^{209}$Bi,X)$^{196}$Au reaction at 1 GeV/u is 3.2±0.2 b while the WW calculation gives a value of 4.2 b. A straight-line-fit to the data points (dashed line in Fig.2) gives a $Z^{1.54\pm0.03}$-dependence of the ED cross section, whereas the WW calculation gives a $Z^{1.86}$-dependence.

It may be speculated that the discrepancy for the heavy systems may be due to the excitation of multi-phonon states at higher excitation energies leading to the evaporation of more than one neutron. To include these effects in the calculation we have used a modified WW formalism, described by Llope and Braun-Munzinger [4]. This decreases the calculated 1n-out cross sections for the heavy projectiles by e.g. 10% for the $^{197}$Au($^{209}$Bi,X)$^{196}$Au reaction, but still overestimates the experimental values (see dotted line in Fig.2). For the excess cross-section found experimentally for low-Z projectiles we have presently no plausible explanation.

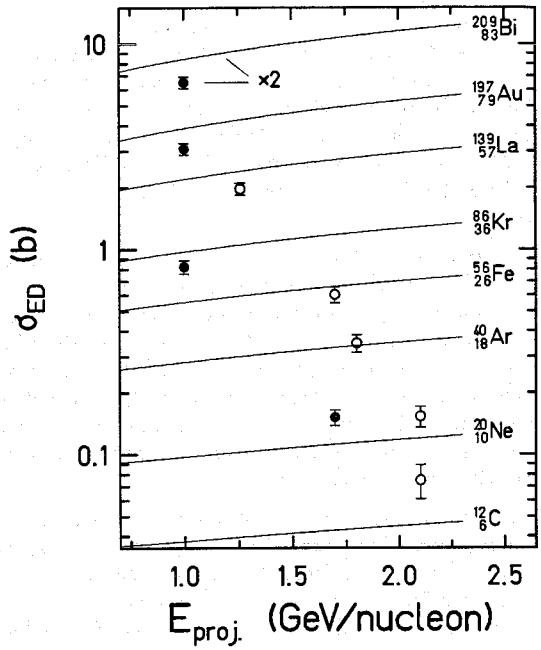


Fig. 1. Experimental ED cross sections for one-neutron removal from a $^{197}$Au target for various projectiles compared to WW calculations (full lines). The open circles are data from Ref.1, the full points are from this work.

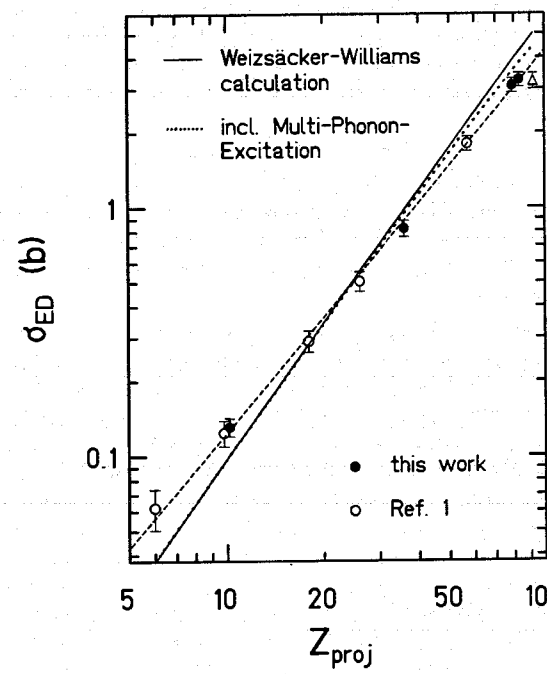


Fig. 2. ED cross sections for one-neutron removal from a $^{197}$Au target as a function of projectile charge. All data points are scaled to the same bombarding energy of 1 GeV/u. The dashed line results from a fit to the experimental data. The recently measured $^{238}$U-point [5] was not included in the fit.

[1] J.C.Hill *et al.*, Phys. Rev. C 38 (1988) 1722 and refs. therein
[2] C.Ziegler *et al.*, GSI Scientific Report 1990, GSI-91-1 (1991) 291
[3] M. Fauerbach *et al.*, Contribution to this Report
[4] W.J.Llope and P.Braun-Munzinger, Phys. Rev. C 41 (1990) 2644
[5] J.C. Hill *et al.*, Phys. Lett. B 273 (1991) 371

# Monitoring of the Total Beam Dose from Au-Foil Activation

Th. Aumann [1], W. Brüchle [2], E. Jäger [2], J.V. Kratz [1], M. Schädel [2]
E. Stiel [1], K. Sümmerer [2], G. Wirth [2]
[1]Institut für Kernchemie, Universität Mainz, [2]GSI, Darmstadt

Cross section measurements for products from the electromagnetic dissociation (ED) of $^{197}$Au-targets after excitation of a giant resonance and subsequent neutron evaporation are discussed in a companion contribution to this report [1]. The ED process leads to very large cross sections for the $^{197}$Au(RHI,X)$^{196}$Au reaction, e.g. 3.2 b for $^{209}$Bi projectiles with energy $E_p$ = 1 GeV/u. The total cross section for the one-neutron removal including the nuclear part is 3.4 b.

Here we report on an off-line method to monitor the total beam dose making use of these now well known, high cross sections as an input. A Au-foil of well known thickness exposed to the heavy ion beam is measured with a calibrated Ge-detector and the residual $\gamma$-activity of $^{196}$Au is determined. The $^{196}$Au half-life of 6 d is very comfortable for activation analysis. It is long enough to avoid early saturation effects and can be used for beam times lasting one or two weeks. On the other hand it is short enough to yield a high enough activity which can easily be measured.

The total 1n-out cross sections in a Au-target are shown in Fig.1 as a function of the projectile charge at an energy of 1 GeV/u. The full points are measured at 1 GeV/u. For all other data the electromagnetic part was scaled to the same energy using the energy dependence as calculated with the Weizsäcker-Williams theory [2]. The nuclear part was determined with an internuclear cascade calculation [3], and the sum of both contributions is depicted in Fig.1. The corrections are less than 15 % of the total cross section.

The solid line in Fig.1 results from a second order polynomial fit to the experimental data. The recent $^{238}$U-point [5] seems to be too low and was not included in the fit. The total 1n-out cross section for any projectile with energy $E_p$ = 1 GeV/u is then given by

$$\sigma_{tot} = a_0 + a_1 Z_p + a_2 Z_p^2$$

with $a_0$ = 61 mb ± 38 mb, $a_1$ = 12.6 mb ± 3.6 mb and $a_2$ = 0.347 mb ± 0.052 mb. The uncertainties of cross sections determined by this method are less than 20 % for $Z_p > 16$ and less than 15 % for $Z_p > 42$. The experimental errors of the measured cross sections are about 6 %.

The target thickness is limited by production of $^{196}$Au from low-energy secondary particles. For a 60 mg/cm$^2$ Au-foil this effect is e.g. 1 % for a 1 GeV/u Au-beam and 4 % for a 1 GeV/u Kr-beam. $^{196}$Au decays to 93 % by electron capture associated with the emission of one 356 keV-photon (64 %) or two photons with energies of 333 keV and 356 keV (23 %). 7 % of $^{196}$Au decays by $\beta^-$ followed by the emission of one 426 keV-photon. When using the strongest, most convenient $\gamma$-line at 356 keV, corrections for coincidence summing of the two gammas or a gamma and X-ray in the detector have to be done in some cases. This correction depends on the total efficiency of the detector and is only important if close detector geometries are needed because of weak activities. It is not necessary if the total number of beam-particles is greater than $10^{10}/\sigma(b)$ for target thickness of 60 mg/cm$^2$. For these higher activities the source shall not be placed on the surface of the detector. Alternatively the 426 keV-line can be used. In most cases no corrections will be needed. To correct for intensity fluctuations during a long activation time a relativ beam intensity monitor is needed.

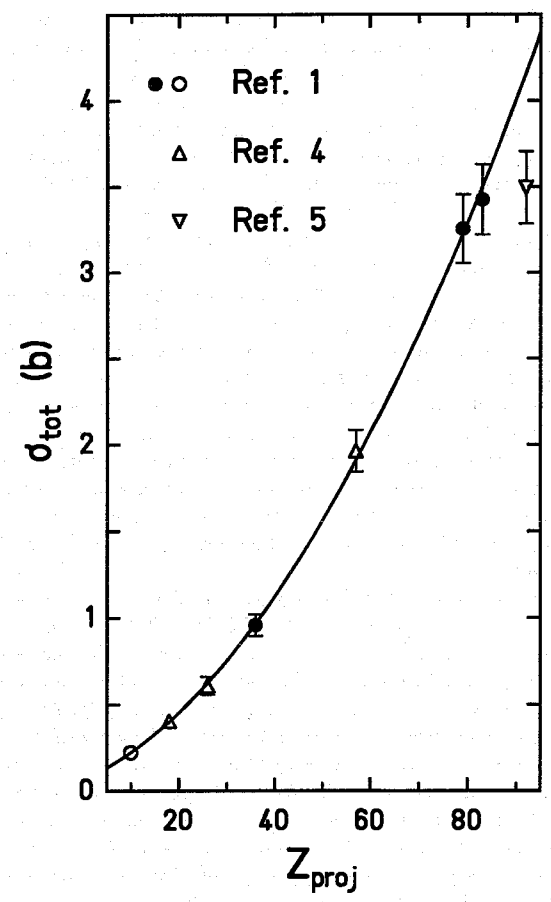


Fig. 1. Total cross sections for the one-neutron removal from a $^{197}$Au target as a function of the projectile charge at an energy of 1 GeV/u. The full points are measured at $E_p$ = 1 GeV/u. All other data points were scaled to the same energy. The solid line results from a second order polynomial fit to the experimental data. The $^{238}$U-point [5] was not included in the fit.

## References

[1] Th. Aumann *et al.*, Contribution to this Report
[2] C.A. Bertulani and G. Baur, Phys. Rep. 163 (1988) 299, J.W. Norbury, Phys. Rev. C 42 (1990) 711
[3] M. Fauerbach *et al.*, Contribution to this Report
[4] J.C. Hill *et al.*, Phys. Rev. C 38 (1988) 1722, and references therein
[5] J.C. Hill *et al.*, Phys. Lett. B 273 (1991) 371

# *Production and Decay of Longer Lived Nuclides of Element 106 for Chemical Investigations*
## *A Feasibility Study*

M. Schädel
GSI Darmstadt

Chemical studies of elements up to Z = 105 have revealed interesting properties [1,2] which may originate from an increasing influence of relativistic effects on the electronic structure.

First model experiments, see contributions to this report, have been made to tailor chemical separations for studies of element 106 properties. The fastest techniques which have been developed up to now need at least more than one second. The longest lived, presently known isotope $^{263}106$ with a half-life of 0.9 s [3] is at the limit of what is detectable. From a cross section of 0.9 nb in the $^{249}Cf(^{18}O,4n)$ reaction [3,4] and typical efficiencies for decay losses during the transport, chemical separation and detection, one may expect to observe between 0.1 and at most 1 atom per hour. This does not exclude chemical studies but will make them extremely time consuming. Therefore it is appropriate to consider the potential of yet unknown nuclei and find out what are supposedly their production cross sections and their decay properties.

The result of a survey of cross section calculations with HIVAP [5] is summarized in Table 1. For the production of $^{264}106$ the reactions $^{248}Cm(^{20}Ne,4n)$ and $^{249}Bk(^{19}F,4n)$ have about equal cross section but a $^{248}Cm$ target is much more advantageous. In spite of the higher cross sections for reactions with $^{254}Es$ targets the presently very limited amount of $^{254}Es$ will yield lower production rates. Consequently, the 4n- and 5n-reactions of $^{22}Ne$ with $^{248}Cm$ are the only choices to produce $^{265}106$ and $^{266}106$. Although all these cross sections for new isotopes are considerably lower than the 0.9 nb for $^{263}106$ a possibly longer half-life of one of these isotopes may nevertheless result in a gain in the observable rate after chemistry.

Table 1: Calculated cross sections for 'n-rich' 106 isotopes

| Isotope | Reaction | Cross Section [pb] |
|---|---|---|
| $^{264}106$ | $^{254}Es(^{14}N,4n)$ | 30 |
| | $^{254}Es(^{15}N,5n)$ | 100 |
| | $^{249}Bk(^{19}F,4n)$ | 20 |
| | $^{248}Cm(^{20}Ne,4n)$ | 10 |
| $^{265}106$ | $^{254}Es(^{15}N,4n)$ | 400 |
| | $^{248}Cm(^{22}Ne,5n)$ | 100 |
| $^{266}106$ | $^{248}Cm(^{22}Ne,4n)$ | 40 |

Estimated EC-, α- and sf half-lives are listed in Table 2. Large uncertainties are not only inherent in the estimates for sf half-lives, where present theoretical calculations are not able to predict half-lives with an accuracy of a factor of ten or better, but also the estimates for α half-lives are quite uncertain. This is because the uncertainty in the $Q_\alpha$ prediction from various mass formulae and the strong dependence of $T_{1/2}(\alpha)$ on this value.

While there is good agreement betweeen experimental results and the masses from Ref.7 for more n-deficient isotopes of the heaviest elements increasingly too high $Q_\alpha$-values result from Ref.7 when going to the most 'n-rich' isotopes. In this region the $Q_\alpha$-values of Ref.8 seem to be a much better choice. The numbers given in Table 2 demonstrate the wide range of α-half-lives based on various $Q_\alpha$ predictions and applying different concepts of half-life calculations.

Table 2: Half-life estimates for 'n-rich' 106 isotopes

| Nuclide | $T_{1/2}$(EC)[a] | $T_{1/2}$(sf) | $Q_\alpha$ (MeV) | Ref. | $T_{1/2}(\alpha)$ | Ref. |
|---|---|---|---|---|---|---|
| $^{264}106$ | 5 min | 10 s[b] | 9.69 | 7 | 8 ms | 10 |
| | | | 9.36 | 11 | 0.3 s | 11 |
| | | | 9.22 | 6 | 0.6 s | 6 |
| | | | 9.00 | 8 | 3.5 s | 9 |
| $^{265}106$ | 4 min | 20 d[c] | 9.55 | 7 | 50 ms | 10 |
| | | | 9.04 | 6 | 24 s | 6 |
| | | | | | 13 s | 9 |
| | | | | | 2 s | 10 |
| | | | 8.68 | 8 | 200 s | 9 |
| | | | | | 28 s | 10 |
| $^{266}106$ | 30 min | 1 h[b] | 9.43 | 7 | 45 ms | 10 |
| | | | 8.90 | 6 | 6 s | 6 |
| | | | 8.85 | 11 | 10 s | 11 |
| | | | 8.46 | 8 | 200 s | 9 |

a) from [6] b) from [12] c) $\frac{T_{1/2}(264) + T_{1/2}(266)}{2} \times 10^3$

Combining all cross section and half-life estimates one is tempted to conclude that an α-decaying $^{265}106$ produced in a $^{248}Cm(^{22}Ne,5n)$ reaction would be the best candidate for chemical studies of element 106. In spite of the low cross section of 0.1 nb an expected half-life of several seconds or longer will result in a significantly increased rate of observed atoms after chemistry compared to $^{263}106$.

1. J.V. Kratz et al., Radiochim. Acta 48, 121 (1989)
2. H.W. Gäggeler et al., Report PSI-PR-91-32(1991)
3. A. Ghiorso et al., Phys. Rev. Lett. 33, 1490 (1974)
4. V.A. Druin et al., Sov. J. Nuc. Phys. 29, 591 (1979)
5. W. Reisdorf, M. Schädel, Z. Phys. A, in press
6. N.N. Kolesnikov, A.G. Denin, VINITI Dep. No. 7309-387 (Tomsk, 1987)
7. S. Liran, N. Zeldes, At. Data Nucl. Data Tables 17, 431 (1976)
8. P. Möller, J.R. Nix, At. Data Nucl. Data Tables 39, 213 (1988)
9. D.N. Poenaru, M. Ivascu, J. Physique 44, 791 (1983)
10. V.E. Viola, G.T. Seaborg, J. Inorg. Nucl. Chem. 28, 741 (1966)
11. Z. Patyk, A. Sobiczewski, Nucl. Phys. A533, 132 (1991)
12. Z. Patyk et al., Nucl. Phys. A502, 591c (1989)

## Nucleon Transfer Reactions and the Electron-Positron Puzzle

H.J. Wollersheim, G. Wirth (GSI Darmstadt)

The detection of narrow lines in electron-positron sum-energy spectra after heavy-ion collisions is experimentally well established. Excitation functions and angular distributions have been measured for the coincidence lines. In the particular case of the $^{238}U + ^{181}Ta$ collision system [1,2], the pair emission probability for the 748 keV sum-energy line shows an exponential increase with decreasing radial separation between the two heavy ions, typically for nuclear reactions in peripheral collision. On the other hand, the line appears only in a very narrow beam energy region (5.93-6.16 MeV/u). This sharp energy dependence reflects a resonance or threshold like effect which has not been found in transfer reactions. Similar results have been obtained for other heavy-ion reactions, however, no conceivable explanation has been given until today although many different attempts have been made.

One-neutron transfer is a main reaction channel in heavy-ion collisions at energies near the Coulomb barrier. Although the collision dynamics of very heavy ions is dominated by the strong Coulomb repulsion, the strong localisation of nucleon transfer reactions at the turning point of a classical trajectory might be used to search for deviations from Rutherford trajectories due to the nuclear interaction potential. Therefore angular distributions for one-neutron transfer in $^{238}U + ^{197}Au$ collisions [3] were measured at 15 different beam energies near and below the Coulomb barrier. Fig.1 shows for the 1n-transfer product $^{196g}Au$ the ratio of the cross section to the Rutherford cross section as a function of the distance of closest approach D. In Ref.3 only neutron transfer probabilities from trajectories with $D > 18.6$ *fm* were analysed and no deviations from Coulomb trajectories were found. The solid line is calculated from the elastic scattering of a nearly identical heavy-ion system, $^{206}Pb + ^{232}Th$ , using a new semiclassical formula [4]. This relationship between elastic scattering and transfer reactions assumes Rutherford trajectories for the collision partners. Even at $D < 18$ *fm* the data are in good agreement with the calculated values. However, a closer inspection of the data - as demonstrated by the linear plots in fig.2 - shows a significant excess of cross section for distance of closest approaches D = 16-17 fm at low bombarding energies (top) relative to the ones above 6.06 MeV/u (bottom). The experimental uncertainties of the 1n-transfer cross sections are typically 5% for the close collisions. The observed cross section excess amounts to about 20 mb measured at internuclear distances which can only be reached in reactions with bombarding energies higher than 5.9 MeV/u.

It is interesting to note, that the energy window of 5.9-6.06 MeV/u for the detection of the additional 1n-transfer cross section almost coincides with the one of the maximum electron-positron pair emission probability of the 748 keV line in the $^{238}U + ^{181}Ta$ system. Since the excitation functions and the angular distributions are very similar, one may raise the question if both observables, nucleon transfer and electron-positron coincidences, study the same physical phenomena.

If the excitation of a nuclear state in the projectile or target nucleus is the physical origin, a cross section of $\simeq 40 \mu b$ for internal pair conversion of a single nuclear transition can be calculated from the additional transfer cross section. This cross section is of the same order of magnitude as the one measured for $e^- e^+$ coincidences although it is difficult to explain the narrow width of the sum lines for a moving emitter. Conversion electron measurements are planned for the $^{238}U + ^{181}Ta$ system in order to clarify this possibility. It might also be possible that longer contact times ($\simeq 10^{-21}$ sec) due to the influence of the nuclear interaction on the trajectory are responsible for the larger transfer cross sections.

1. P. Salabura et al.,Phys.Lett.245B,153 (1990)
2. H. Bokemeyer,W. König, Int.Conf.on Nucl.Phys.,Brioni,1991
3. G. Wirth et al., Phys.Lett.253B,28 (1991)
4. H.J. Wollersheim et al., GSI scientific report 1991

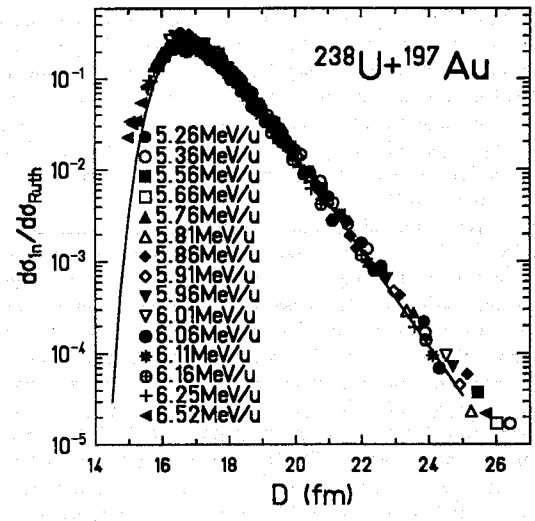


Fig. 1: Ratio of the 1n-transfer cross section to the Rutherford cross section for the $^{238}U + ^{197}Au$ system as a function of the distance of closest approach.

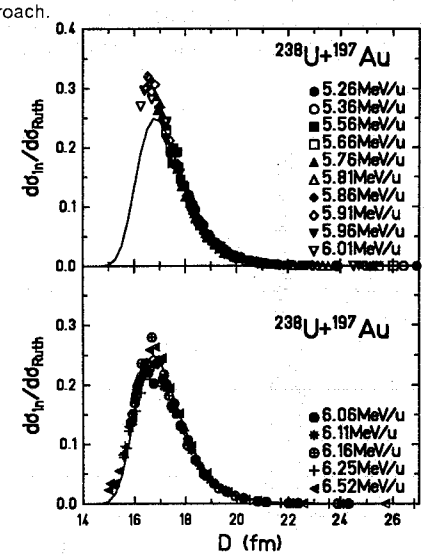


Fig. 2: Linear representation of the same data as shown in fig.1 for incident energies below (top) and above (bottom) 6.03 MeV/u. The solid line is calculated from a semiclassical relationship between elastic scattering and transfer reactions [4].

# Observation of Surface Tracks in an Amorphous Metal

C. Trautmann, S. Andler, W. Brüchle, R. Spohr, (GSI Darmstadt)
M. Toulemonde (CIRIL, Caen)

## Introduction

Since a long time it has been known that electronic excitation and ionization arising from the electronic energy loss of energetic ions may induce latent tracks in insulators. Until recently it was commonly assumed that no effect of this kind could exist in metallic alloys, since the high density and mobility of free electrons would smear out any electronic perturbation instantaneously. Lately high energy heavy ion irradiation of a large variety of metallic alloys [1-4] has nevertheless proven that structural changes due to electronic energy loss occur in metallic systems. For metallic alloys in an amorphous state the following effects were observed:

1) An increase of the electrical resistance [3].
2) Dramatic sample growth perpendicular to the ion beam without volume change above an incubation fluence [4].
3) As in the case of insulators an electronic stopping power threshold also exists for metals.

The mechanism of damage creation by electronic excitation in metallic compounds is still open. The electron mobility [5] and the existence of soft phonon modes [6] may play an important role.

The immediate question in the context of structural applications was if these highly damaged zones could be selectively etched by a sufficiently soft chemical agent leaving the matrix intact. Here we report on first experiments trying to produce pores by etching metallic samples irradiated by heavy ions.

## Experimental

We irradiated 25 to 30 μm thick samples of the amorphous metal $Fe_{81}B_{13.5}Si_{3.5}C_2$ through a hexagonal mask with gold ions of 13.4 MeV/u at the GSI Unilac and with uranium ions of 11.8 MeV/u at GANIL. The corresponding maximum linear energy transfer was 5.1 keV/Å and 6.3 keV/Å, respectively. The irradiated samples were etched in 0.04 n $FeCl_3$ solution at room temperature for one hour.

## Results

After the etching the structure of the irradiation mask was visible already by the naked eye. This is a rough indication that the etchant is capable to distinguish between irradiated and not irradiated areas. Another macroscopic observation was the increased brittleness of the etched samples. A closer look at the irradiated zones with the SEM revealed surface tracks in the form of conical etch pits with an opening angle around 55°. The masked zones of the sample stayed flat, confirming that the creation of etch pits is associated with the irradiation.

Conical etch pits were observed only for samples that were irradiated in the direction of the surface normal. Accordingly, the cones were always symmetrical. Further irradiations with tilted ion beams are needed in order to distinguish between surface and volume effects.

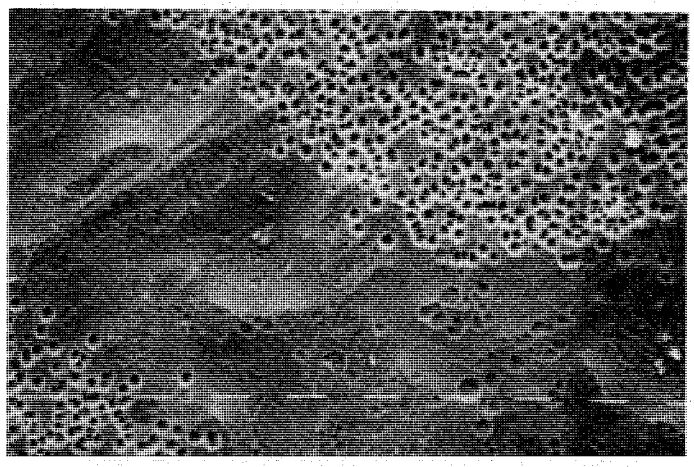

Fig. 1. SEM-picture of surface pores. Irradiated and masked areas can be clearly distinguished (scale bar: 10 μm).

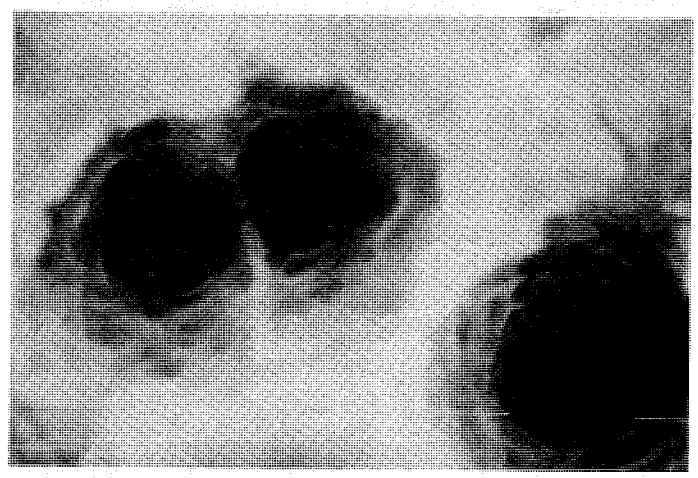

Fig. 2. Surface pores of about 2 μm diameter and depth (scale bar: 1 μm)

[1] A. Barbu et al, Europhys. Lett. **15**, p. 37 (1991)
[2] A. Audouard et al, Phys. Rev. Lett. **65**, p. 875 (1990)
[3] A. Audouard et al, Europhys. Lett. **5**, p. 241 (1988)
[4] Ming-dong Hou et al, Phys. Rev.B, 41, p. 1144 (1990)
[5] M. Toulemonde et al, to be published in Phys. Rev.
[6] A. Dunlop et al, Europhys. Lett. **15**, p. 765 (1991)

# Etching of Particle Tracks in Kapton

C. Trautmann, W. Brüchle, R. Meyer, R. Spohr, J. Vetter, N. Angert (GSI Darmstadt)

## Introduction

The polyimide Kapton® stands out for its unique combination of mechanical, electrical and thermal strength which makes it an interesting candidate for particle track applications. However, until recently, track etching in Kapton gave unsatisfactory results such as broad pore size distributions [1] and irreproducible pore geometries. The clue for dramatically improving track etching in Kapton was found in the precise control of the pH of the etchant (NaOCl).

## Experimental

The irradiations were performed at the Unilac with gold ions at a specific energy of 11.4 MeV/u. The initial active chlorine content of the NaOCl was 13% and the initial pH was 12.3. In order to optimize track etching the pH was varied systematically. The track etch rates were determined in an electrolytic conductivity cell in which the break-through of individual single-pores could be observed [2].

## Results and discussion

Bulk etch rates

The bulk etch rate $v_b$ was determined from the decrease of the foil thickness for several pH values. It depends exponentially on pH (Fig.1).

$v_b = 2.1 \cdot 10^{-5} \exp(0.82 \cdot \mathrm{pH})$, at T=58°C.

The temperature dependence of the bulk etch rate was determined at pH=10 in the temperature range between 45 and 75° C in which it follows the Arrhenius equation

$v_b = 2.4 \cdot 10^{8} \exp(-E_a/kT)$, at pH=10,

where $E_a$=0.63 eV is an activation energy.

Track etch rate

In contrast to the exponential increase of the bulk etch rate the track etch rate $v_t$ shows a linear dependence on the pH of the etchant (Fig.2):

$v_t = -4.0 + 0.48 \cdot \mathrm{pH}$, at T=58°C.

Pore geometry

The surface of the etched Kapton foil shows regularly shaped circular pores. Even after several hours of etching no roughness of the pore walls was observed. The pore geometry is a function of the track etch ratio, $v_b/v_t$. For low pH very small cone angles can be obtained while for high pH the pores show opening angles of up to 30° (Fig.3).

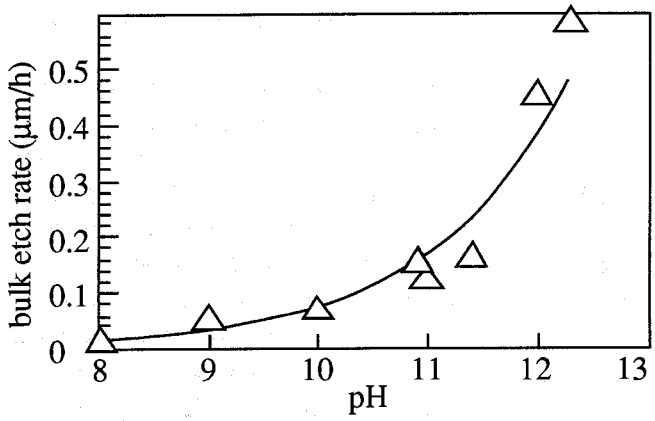


Fig. 1 Bulk etch rate of Kapton versus pH of NaOCl.

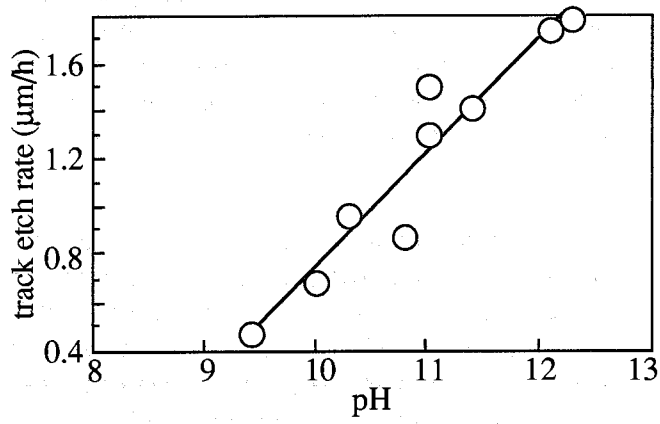


Fig. 2 Track etch rate of Kapton versus pH of NaOCl.

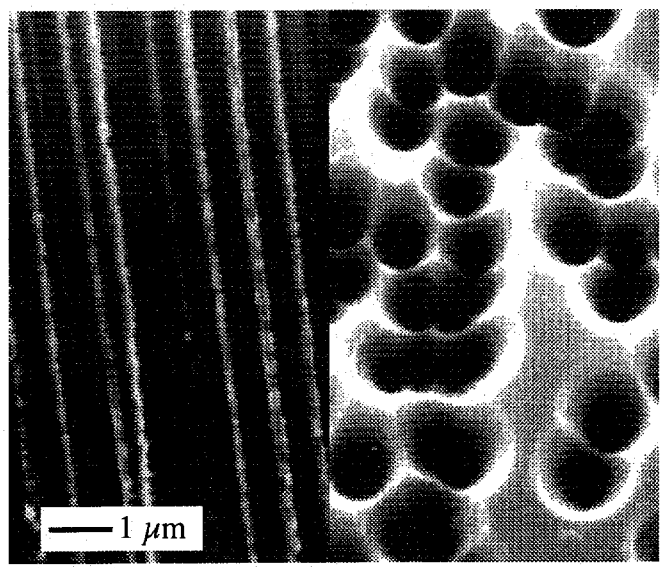


Fig. 3 Left: cross section of pores etched at pH 9 Right: funnel shaped pores etched in NaOCl at pH 12.3,.

[1] S. Heise, Diplomarbeit Kernchemie Marburg (1990).
[2] C. Trautmann et al., GSI Report 88-1, p. 246, 1988.

## *Fast Tungsten Separations with ARCA as a Test for the Chemical Characterization of Element 106*

W. Brüchle, B. Schausten, E. Jäger, E. Schimpf, M. Schädel
GSI Darmstadt
J.V. Kratz, N. Trautmann, H.P. Zimmermann
Institut für Kernchemie, Universität Mainz
H. Bruchertseifer, W. Heller
Zentralinstitut für Isotopen- und Strahlenforschung, Leipzig

The Automated Rapid Chemistry Apparatus, ARCA [1], has successfully been applied to study the behaviour of element 105 in aqueous solution [2], and to search for the new isotope $^{263}$Ha [3]. As a complementary method to the fast centrifuge system SISAK [4,5] we have tested the capability of ARCA to study chemical properties of element 106 with the 0.9 s $^{263}$106 or the presumably accessible and longer lived isotope $^{265}$106 [6].

Tungsten as the element 106 homologue in group 6 has been produced in a $^{20}$Ne + $^{nat.}$Gd reaction together with the group 3, 4 and 5 elements Lu, Hf and Ta. All products have been transported with a He/KCl-cluster jet to ARCA. Differences in complex formation in aqueous solution have been applied for chromatographic separations with a strong cation exchange resin (17.5 ± 2 µm Aminex A6) in 1.6 x 6 mm columns at room temperature. Flow rates were kept at 1 ml/min.

In first experiments, α-hydroxyisobutyric acid ( α-HIB ) solutions of various concentrations and pH-values have been tested, see Table 1. While in all solutions W has been eluted quantitatively within 120 µl, Lu as a typical group 3 element has been found in the effluent at a level of less than 1 % ( the sensitivity in our experiment ), and 4 % Hf have been observed for the two lowest concentrations. Unbuffered 5 x $10^{-2}$ M α-HIB with a pH of 2.65 and buffered solutions with pH-values of up to 5 provide a good separation of the actinide and element 104 homologues Lu and Hf from the 106 homologue W.

Table 1: Separation of Lu and Hf from W

| | Percentage of initial activity in W fraction | |
|---|---|---|
| Aqueous solution | Lu | Hf |
| α-HIB, 1x$10^{-4}$ M, pH=4.04 | <1 | 4±4 |
| α-HIB, 1x$10^{-3}$ M, pH=3.34 | <1 | 4±4 |
| α-HIB, 5x$10^{-2}$ M, pH=2.65 | <1 | <1 |
| α-HIB, 5x$10^{-2}$ M, pH=5 | <1 | <1 |
| 0.1 M HCl | <1 | <1 |
| 0.1 M HCl / 1x$10^{-5}$ M HF | <1 | <1 |
| 0.1 M HCl / 1x$10^{-4}$ M HF | <1 | <1 |
| 0.1 M HCl / 5x$10^{-4}$ M HF | <1 | <1 |
| 0.1 M HCl / 7.5x$10^{-4}$ M HF | 28 | 3 |
| 0.1 M HCl / 1x$10^{-3}$ M HF | 80 | 75 |
| 0.1 M HCl / 1x$10^{-2}$ M HF | 80 | 8 |
| 1x$10^{-2}$ M HF | 80 | 8 |

As an alternative to organic complexing agents, various concentrations of HF in 0.1 M HCl have been investigated. Again for all solutions listed in Table 1 the W elution was complete. Good separations of W from Hf and Lu can only be achieved for HF concentrations below 7.5 x $10^{-4}$ M. In all systems investigated Ta has not been separated from W. Presently, we are considering this to cause no problem because element 105 isotopes, if any produced, will most likely not interfere with the element 106 isotope identification.

The elution curve depicted in Fig. 1 shows the speed of the separation. From this result we can expect to obtain an element 106 fraction with a yield of 85 % within about 50 µl. This corresponds to a time of about 3 s and is in agreement with the results from experiments on element 105 [7].

For experiments on element 106 isotopes with half lives of a few seconds or more which may be accessible in future nuclear reactions [6] the ARCA technique is very well suited.

1. M. Schädel et al., Radiochim. Acta 48, 171 (1989)
2. J.V. Kratz et al., Radiochim. Acta 48, 121 (1989)
3. J.V. Kratz et al., Preprint GSI 91-32 (1991)
4. H. Persson et al., Radiochim. Acta 48, 177 (1989)
5. F. Haberberger et al., contrib. to this report
6. M. Schädel, contribution to this report
7. M. Schädel et al., Preprint GSI 92-04 (1992)

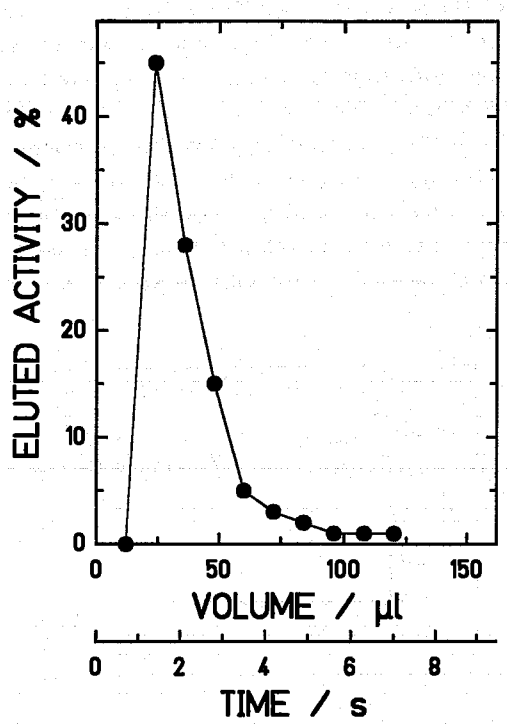


Fig.1: Elution of W activity in ARCA from Aminex A6 with α-HIB and HCl/HF

## *Sorption of Carrier-free W-, Hf- and Lu-Isotopes on Strongly Acidic Cation Exchangers* G+B

S. Fischer[1], A. Roß[1], W. Brüchle[2], E. Jäger[2], B. Schausten[2], M. Schädel[2], H. Bruchertseifer[3]
[1] Technische Universität Dresden, [2] GSI Darmstadt, [3] Zfl Leipzig

***Introduction:*** The cations of W, Hf and Ta tend to hydrolyze already in weak acid solution and form different polyhydrolysates depending on the metal concentration, pH and anion[1]. Only at trace concentrations, the formation of mononuclear hydrolysis products can be determined. Hydrolysis can be repressed by strong complexing agents, e.g. fluoride anions [2-4]. This effect can be used to define the chemical state of an ion as well as for the development of model conditions for the separations of new elements[5,6].

***Experimental:*** All nuclides were obtained by heavy ion reaction ($^{nat}$Gd + $^{20}$Ne) from the UNILAC at the GSI Darmstadt. The trace elements were collected after transport with a KCl-gas jet on a frit and after defined times (15-20 min) eluted by selected fluorid solutions. Distribution coefficients were determined by batch experiments at 298 K. Aliquots from the solutions were taken after shaking for defind times and γ-activity was measured:

| | | |
|---|---|---|
| $^{170}$W: | $T_{½}$ = 2.4 min | 124.7, 316.2 keV |
| $^{166}$Hf: | 6.77 min | 78.8 keV |
| $^{168}$Hf: | 25.5 min | 183.8 keV |
| $^{169}$Hf: | 3.25 min | 492.9 keV |
| $^{168m}$Lu: | 6.7 min | 198.8 keV |
| $^{166}$Lu: | 2.6 min | 1459.6 keV |
| $^{165}$Lu: | 11.8 min | 120.6 (203.6) keV |

These measured γ-energies coincide with literature data[7,8] (ΔE = 0.5 keV). Cation exchanger of the KPS-type (Bitterfeld AG, FRG; comparable to Dowex 50x8) of 200 mesh or 40-50 mesh was used. For each solution 3-4 experiments were carried out.

***Results and discussion:*** Sorption experiments were carried out from solutions with constant ionic strength (0.5 M HCl/$HClO_4$) and different HF concentrations (comparable conditions to ARCA studies) [6]. By repeated ion exchange with fresh solution and studies with resins of different particle size reversible and reproducible data were obtained. Fig. 1 shows the detected percentages of trace ions in the solutions as a function of time.

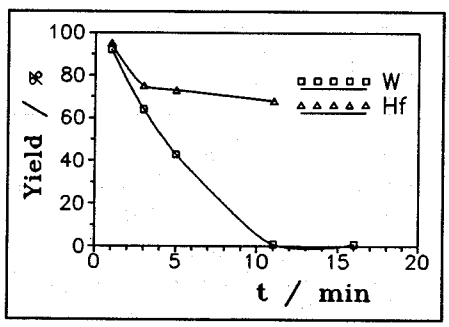


***Fig.1:*** Percentage of trace ions in solution as a function of time (200 mg KPS 200, 5 ml solution: 0.5 M HCl/$10^{-4}$ M HF) at 298 K

Differences in sorption rates and kinetics are to be seen. While for Hf equilibrium is obtained after short time (3-5 min; nearly 65 % remains in solution) W requires a longer shaking time before it is completely sorbed. Lu as a model for actinides is sorbed at > 99 % after 1 min, the shortest time tested in our experiments. A shaking time of 3 or 5 min was selected for further experiments. Table 1 shows some distribution coefficients D(ml × $mg^{-1}$).

***Table 1:*** Distribution coefficients (lg D) after a shaking time of 3 min (or 5min)

| | 0.5 M HCl $10^{-4}$ M HF | 0.5 M HCl $10^{-3}$ M HF | 0.5 M $HClO_4$ $10^{-4}$ M HF | 0.5 M $HClO_4$ $10^{-3}$ M HF |
|---|---|---|---|---|
| W | 1.2±0.1 | -0.19 | 0.9±0.1 | 0.5±0.1 |
| Hf | 1.0±0.1 | -0.04 | 1.2±0.1 | -0.04 |
| Lu | >3.4 | >3.4 | >2.9 | >2.9 |

Good separation conditions are to be observed in $HClO_4$ solution at low HF concentration. Experiments in alkaline solution (0.01 M NaOH) were not successful because of irreversible adsorption of hydrolysis products. Our results seem to be partly in contradiction to results from dynamical methods especially to high speed ARCA separations [6]. These differences may be due to nonequilibrium conditions.

***Conclusions:*** From the above discussed results experimental conditions for reversible distributions were deduced. The experiments should be continued in order to determine complex stability and hydrolysis data in fluorid containing solutions and to find conditions for an effective separation. Elements like Zr, Nb, Pa and Mo should be included into model studies for very heavy elements. These experiments are to be applied to dynamical methods with slow elution rates and high speed methods used for example in the ARCA II.

1. C.F. Baes, R.E. Mesmer: The Hydrolysis of Cations, Wiley-Interscience-Publ., New York, London, Sydney 1976
2. E. Högfeld (Editor): Stability Constants of Metal-Ion-Complexes, IUPAC Chem. Data Series No. 21, Pergamon Press, London 1982
3. H. Bruchertseifer, Promotion B, Leipzig 1982
4. M. Marhol: Ion Exchangers in Analytical Chemistry, Akademia, Prag 1982
5. H. Bruchertseifer, Zfl-Mitteilungen 165, 6 (1991)
6. W. Brüchle et al., contrib. to this report
7. G. Erdtmann, W. Soyka: The Gamma Rays of the Radionuclides, Verlag Chemie, Weinheim 1969
8. Recherche, STN-Datenbank Karlsruhe, File INNIS, 1988-1991 (Nuclear Data for $^{170-172}$W, $^{166-170}$Hf, $^{166-170}$Ta)

# Separation of Tungsten by Liquid-Liquid-Extraction with SISAK 3 as a Test for Chemical Studies of Element 106

F. Haberberger, M. Pense-Maskow, G. Herrmann, A. Nähler, N. Trautmann
Institut für Kernchemie, Universität Mainz
M. Schädel
GSI Darmstadt
J. Alstad
Department of Chemistry, University of Oslo
G. Skarnemark
Chalmers University of Technology, Göteborg

To develop fast and continuous chemical separation procedures for the elements 103, 104, 105 and 106 by liquid-liquid extraction with the centrifuge system SISAK 3 [1], the lighter homologues have been used as tracers, assuming that there is a similarity in the chemical behaviour.
The homologues of the heaviest elements have been produced by thermal neutron induced fission of $^{239}Pu$ and in the bombardement of natural gadolinium with $^{20}Ne$-ions. The products have been transported with a gas jet to SISAK 3 where the fast liquid-liquid-extractions have been carried out.
The extraction of lanthanides, zirconium, hafnium, niobium, tantalum, molybdenum and tungsten in tricaprylamine (Alamine-336), trioctylamine, tricapryl-methyl-ammonium-chloride (Aliquat-336), tributylphosphinoxide (TBPO), trioctylphosphinoxide (TOPO) and tributylphosphate (TBP) from various inorganic acid solutions have been investigated.
As an example Figure 1 shows the extractions into Aliquat-336 from hydrochloric acid.

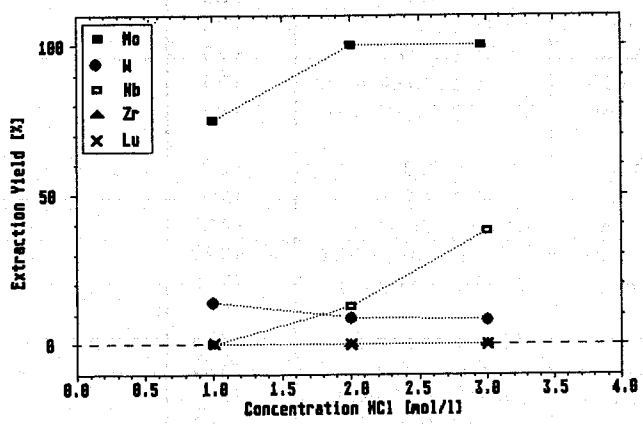


Figure 1 : Extraction of molybdenum, tungsten, niobium, zirconium and lutetium from HCl into Aliquat-336/toluene

No or almost no extraction of lanthanides, zirconium, hafnium, niobium, tantalum, and tungsten into the organic phase could be observed, whereas molybdenum is extracted almost quantitatively at higher HCl concentrations.
With TOPO in Shellsol-T [50 g/l] the best results for the separation of tungsten have been obtained.
From 4 M HCl 95 % of tungsten are extracted into the organic phase, while more than 85 % of tantalum, hafnium and lutetium remain in the aqueous phase as it is illustrated in Figure 2.
The yields for the fission homologues are given in Figure 3.
From these data one can conclude the best conditions for the chemical separation of element 106 with SISAK 3 is the extraction into TOPO/Shellsol-T from 3-4 M HCl.

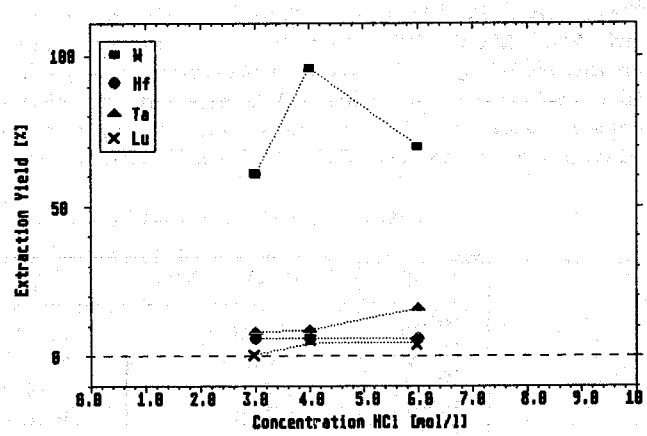


Figure 2 : Extraction of tungsten, tantalum, hafnium and lutetium from HCl into TOPO/ Shellsol-T

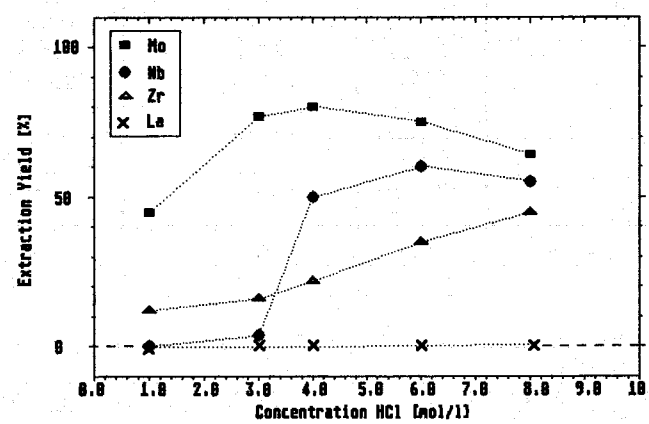


Figure 3 : Extraction of lanthanum, niobium, zirconium and molybdenum from HCl into TOPO/Shellsol-T

1. H. Persson et al., Radiochimica Acta 48, 177 (1989)

# Half-Lives of Short-Lived W-, Ta- and Hf-Isotopes as Determined in Model Experiments for the Chemical Separation of Element 106 B,G

W. Heller[1], R. Binder[1], H. Bruchertseifer[1], U. Becker[2], F. Haberberger[2], G. Herrmann[2], J. V. Kratz[2], M. Mendel[2], A. Nähler[2], M. Pense-Maskow[2], N. Trautmann[2], N. Wiehl[2], W. Brüchle[3], E. Jäger[3], M. Schädel[3], B. Schausten[3], J. Alstad[4], G. Skarnemark[5], R. Dressler[6], S. Fischer[7], A. Roß[7], B. Eichler[8], S. Hübener[8]

[1]Zentralinstitut für Isotopen und Strahlenforschung, Leipzig, [2]Institut für Kernchemie, Universität Mainz, [3]GSI Darmstadt, [4]Department of Chemistry, University of Oslo, [5]Chalmers University of Technology, Göteborg, [6]Universität Leipzig, [7]Technische Universität Dresden, [8]Zentralinstitut für Kernforschung, Rossendorf

Fast chemical procedures have been applied for the separation and detection of short-lived neutron-deficient W-isotopes from complex nuclear reaction mixtures, assuming that the behaviour of element 106 is similar to tungsten. Experiments have been performed with the SISAK 3-system [1] using liquid-liquid-extractions and ion-exchange separations, with ARCA [2,3] utilizing chromatographic separations with a strongly acidic cation exchange resin and also with gaschromatographic techniques [4].

The W-isotopes were produced in the $^{nat}$Gd ($^{20}$Ne, xn) reaction with beam energies of 170 and 207 MeV. The reaction products were transported by a He/KCl gasjet to the separation units and the isolated tungsten fractions were measured with HP-Germanium detectors (planar and coaxial). SISAK 3 and ARCA were used to detect the short-lived isotopes, whereas the longer-lived isotopes were covered by the gaschromatographic technique.

For the half-life determinations of the neutron-deficient W-isotopes and their decay products the $\gamma$-ray singles spectra were recorded in preselected time sequences.

The evaluated values are summarized in Table 1 together with literature data. As can be seen W-isotopes with mass numbers 171 to 166 could be identified as well as Ta- and Hf-isotopes from A = 170 to 162. The measured half-lives are in good agreement with the published data. The half-lives of $^{164}$Hf (1.77 ± 0.3 min) and $^{165}$Hf ( 1.28 ± 0.07 min ) are in accordance with [5]. These results will serve as a database for further experiments to optimize the fast chemical separations for the investigation of the very short-lived W-isotopes.

Table 1: Half-lives of neutron-deficient W-, Ta- and Hf-isotopes

| Isotop | Energy [keV] | $T_{1/2}$ exp | $T_{1/2}$ lit | Ref. |
|---|---|---|---|---|
| $^{166}$W | 125.8 | 22..0 ± 1.0 s | 18.8 ± 0.4 s | [5] |
| $^{167}$W | 110.2 | 23.0 ± 6.0 s | 19.9 ± 0.5 s | [6] |
| $^{168}$W | 178.5 | 46.9 ± 3.0 s | 53.0 ± 2.0 s | [7] |
| $^{169}$W | 169.5 | 80.0 ± 6.0 s | 76.0 ± 6.0 s | [7] |
| $^{170}$W | 316.2 | 2.8 ± 0.1 min | 2.42 ± 0.04 min | [7] |
| $^{171}$W | 478.7 | 2.5 ± 0.2 min | 2.38 ± 0.04 min | [7] |
| $^{164}$Ta | 210.7 | 15.5 ± 2.0 s | 14.9 ± 0.2 s | [8] |
| $^{166}$Ta | 158.7 | 31.5 ± 5.0 s | 32.0 ± 3.0 s | [9] |
| $^{167}$Ta | 278.0 | 80.0 ± 4.0 s | 80.0 ± 20.0 s | [10] |
| $^{170}$Ta | 55.8 | 7.2 ± 0.7 min | 6.76 ± 0.06 min | [14] |
| $^{171}$Ta | 49.6 | 22.7 ± 2.0 min | 25.0 ± 2.0 min | [11] |
| $^{162}$Hf | 173.9 | 38.0 ± 9.0 s | 37.6 ± 0.8 s | [12] |
| $^{163}$Hf | 71.0 | 40.0 ± 8.0 s | 40.0 ± 0.6 s | [12] |
| $^{164}$Hf | 122.1 | 1.77 ± 0.3 min | 1.85 ± 0.13 min | [5] |
| | | | 2.8 ± 0.2 min | [13] |
| $^{165}$Hf | 179.9 | 1.28 ± 0.07 min | 1.27 ± 0.07 min | [5] |
| | | | 1.70 ± 0.1 min | [13] |

1. H. Persson et al., Radiochim. Acta 48, 177 (1989)
2. M. Schädel et al., Radiochim. Acta 48, 171 (1989)
3. S. Fischer et al., contribution to this report
4. S. Hübener et al., contribution to this report
5. T. Hild et al., Nucl. Phys. A492, 237 (1989)
6. F. Meissner et al., Z. Phys. A. 332, 153 (1989)
7. F. Meissner et al., Z. Phys. A. 337, 45A (1990)
8. E. Runte et al., Z. Phys. A. 324, 119 (1986)
9. R. E. Leber et al., J. Inorg. Nucl. Chem. 39, 927 (1977)
10. H. Bruchertseifer et al., Radiochim. Acta 47, 941 (1989)
11. I. Rezanka et al., Phys. Rev. Lett. 25, 1499 (1970)
12. U. J. Schrewe et al., Phys. Rev. C25, 3091 (1982)
13. H. Bruchertseifer et al., Radiochem. Radioanal. Lett. 48, 391 (1981)
14. R. E. Leber et al., J. Inorg. Nucl. Chem. 38, 951 (1976)

# $MoO_3$ as a new cluster material for a gas-jet

H.U. Becker, J.V. Kratz
Institut für Kernchemie, Universität Mainz

H. Gäggeler, D. Jost, J. Kovacs, A.Weber
PSI, Villigen, Switzerland

M. Schädel, W. Brüchle, E. Jäger, E. Schimpf
GSI, Darmstadt

The gas phase chemistry in a $O_2/H_2O$ environment may open a path to study the chemical behaviour of element 106 with acidic hydrated oxides [1]. But it can be prohibitive for these experiments to use KCl as a cluster material in the gas-jet because of the formation of KOH at higher temperature, which prevents the formation of volatile $MO_3$ and $M(OH)_2O_2$ compounds [2]. Therefore, for use as an alternative cluster material, we have studied the behaviour of $MoO_3$.

Fission products from the "SAPHIR" reactor at the PSI have been transported at a He flow-rate of 2.8 l/min and a pressure of 1.0 bar through a 130m long capillary (ø2mm) from the target-chamber to the counting station [3]. The transportation yield with $MoO_3$ has been determined through $\gamma$-spectroscopy of fission products relative to the well known yield of a KCl-jet [3].

In a Differential mobility analyzer (DMA) where charged clusters are separated by an electrical field perpendicular to the direction of the gas-flow and an optical particle counter called Condensation Nuclei Counter (CNC), the diameter, the surface area, and the number of $MoO_3$ clusters have been determined at the end of the capillary [4].

The relative transportation yield as a function of the temperature of the He gas passing over the $MoO_3$ in a standard oven is shown in Fig. 1. Temperatures of 630°C and higher are needed for a good yield. The upper limit to the temperature is set by large amounts of $MoO_3$ material being evaporated at 650°C and above. This is prohibitive because of possible clogging of the capillary or filters and because increasing macro amounts of cluster material are being introduced into the chemistry.

For the interesting temperature range from 550°C to 670°C we have characterized the clusters, see Fig. 2. The total "number" of all particles is drastically increasing up to 600°C and has reached a plateau value of about $4 \cdot 10^6$ particles/cm³ at 640°C. Part of this saturation effect may be due to some experimental limitation in the CNC measurement because only particles smaller than 450 nm can be detected. The total surface of all particles is showing a slightly different behaviour: The total surface is still increasing above 640°C. The increase in particle number and total surface are the dominant effects determining the strong increase in the transportation yield between 580°C and 620°C. The most probable cluster size with about 10 nm diameter at 550°C and 250 nm at 670°C shows a moderate dependence on temperature. But it is important to note that the size distribution is changing more rapidly with a significantly increasing probability for the formation of larger particles. Information about the optimum cluster size for transporting along various distances has to await further analysis.

The stability of the transportation yield over a period of 15 hours is depicted in Fig. 3 for two temperatures. While at 608°C the yield is rather constant, it decreases by about 30% for an oven temperature of 630°C.

From these experiments we can conclude that $MoO_3$ can be used as a cluster material to build an efficient and stable gas-jet transportation system.

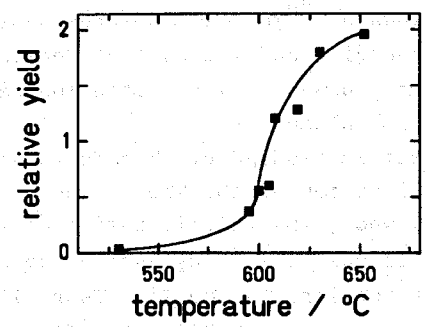


Fig. 1: Transportation yield of the $MoO_3$-jet as the function of the oven temperature

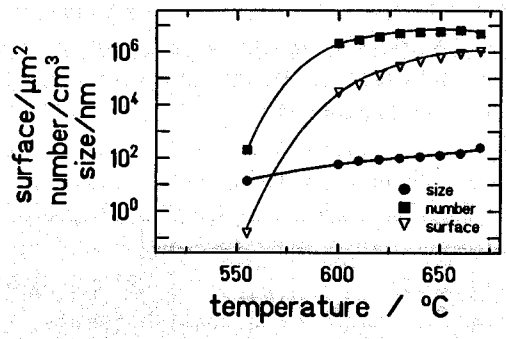


Fig. 2: Number, size and surface of $(MoO_3)_n$-clusters as a function of the oven temperature

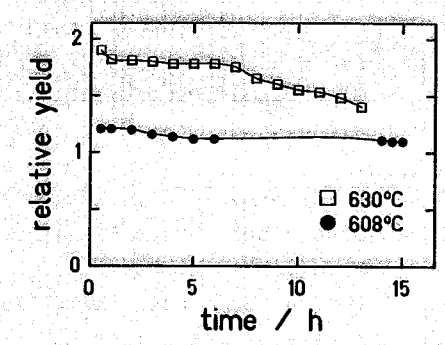


Fig. 3: Time dependence of the $MoO_3$-jet transportation yield for two oven temperatures

[1] S. Hübener et al., contribution to this report
[2] Gmelins handbook of inorganic chemistry, 22, 392 (1938)
[3] H.W. Gäggeler et al., PSI PR-91-15, (1991)
[4] A. Weber, internal report, PSI, TM-32-90-06, (1990), unpublished

## Gaschromatographic Studies of Oxides and Hydroxides of Tungsten B+G

S. Hübener, B. Eichler
Zentralinstitut für Kernforschung Rossendorf
U. Becker, J.V. Kratz
Universität Mainz
H.W. Gäggeler, D.T. Jost, J. Kovacs
Paul Scherrer Institut, Villigen, Switzerland
M. Schädel, W. Brüchle, E. Jäger
GSI Darmstadt

In preparation for gaschemistry experiments with element 106 we have studied the gaschromatographic behaviour of short-lived isotopes of W in quartz columns using a mixture of He, $O_2$ and $H_2O$ as the carrier gas.
Isotopes of W were produced at the UNILAC in reactions of $^{20}Ne$ with Gd targets at different energies and transported continuously by a He/$MoO_3$ gas-jet system into the gaschromatography columns.
At first we studied by thermochromatography the collection of the $MoO_3$ aerosols on hot quartz wool, the volatilization of W species from the quartz wool by adding humid oxygen to the carrier gas and the adsorption of the W species on quartz. After a collection time of 30 minutes the distribution of $\gamma$-active nuclides was measured off-line by $\gamma$-spectrometry. A schematic of the set-up and a typical thermochromatogram are shown in Fig. 1. Aerosols and lanthanoides ($^{157}Dy$) were retained completely by the quartz wool at temperatures >1000 K. A total volatilization of W with humid oxygen could not be achieved. At 1250 K only 20% of $^{168}W$ ($T_{1/2}$=53s) and 6% of $^{167}W$ ($T_{1/2}$=19s) were volatilized. Obviously the volatilization proceeds very slowly. By replacing the quartz wool by quartz capillaries the volatilization yield could be increased essentially. From the experimental deposition temperatures $\Delta H_{ads}$=-40±10 kJ/mol and $\Delta S_{ads}$=-11±5 J/molK were evaluated corresponding with the deposition of $WO_2(OH)_{2(g)}$ as $WO_{3(ads)}$.
Fig. 2 shows the experimental set-up for isothermal gaschromatography. Volatile species passing through the column were collected on a glass filter. After a collection time of 120s the activity of the filter was measured off-line by $\gamma$-spectrometry. In a series of experiments the temperature of the quartz wool was varied between 500 K and 1450 K whereas the temperature of the isothermal section was kept constant at about 1070 K. Up to temperatures of 970 K a breakthrough of aerosols was noticed. With increasing temperaure the chemical yield of $^{171}W$ ($T_{1/2}$=2.5 min) could be increased up to 50 % at 1450 K. Fig. 3 depicts the yield of $^{171}W$ as a function of the temperature of the isothermal section whereas the temperature of the quartz wool was kept constant at about 1270 K.
The experiments have to be continued in order to increase the chemical yield further.

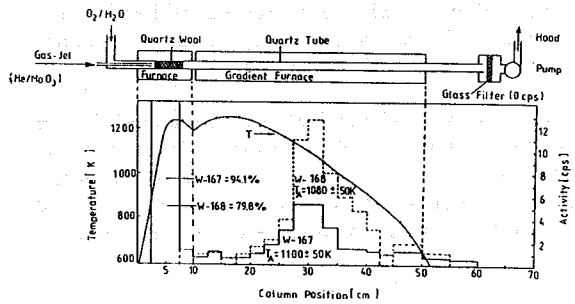


Figure 1: Thermochromatography set-up and distribution of $^{167}W$ and $^{168}W$

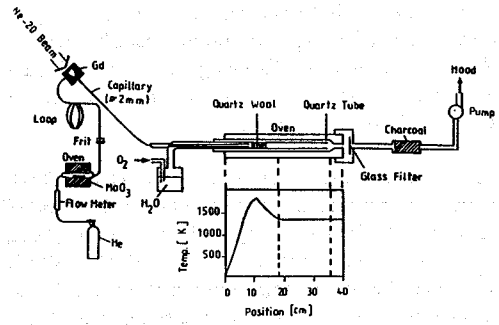


Figure 2: Schematic of the set-up for isothermal chromatography

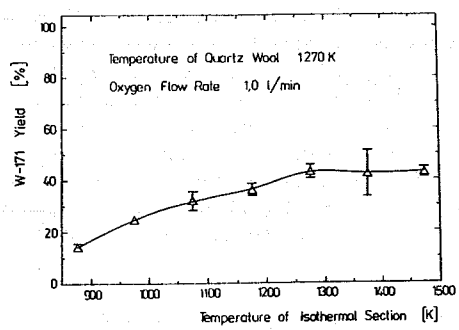


Figure 3: Chemical yields for volatile oxides and hydroxides of $^{171}W$

# On-line isothermal gas chemistry experiments with tungsten chloride

H.W. Gäggeler, D.T. Jost, A. Kovacs
Paul Scherrer Institut, Villigen Switzerland

M. Schädel, W. Brüchle
GSI-Darmstadt

U. Becker, J.V. Kratz
Universität Mainz

B. Eichler, S. Hübener
ZfK-Rossendorf

For possible future experiments with element 106 on-line chemical techniques have to be developed.

In this contribution we describe one possible approach, a continuous separation of volatile chlorides using isothermal gas chromatography. To model an element 106 chemistry its homolog W was used.

A 1.0 mg/cm$^2$ thick Gd target was bombarded with a 170 MeV $^{20}$Ne beam at the UNILAC accelerator to produce the short-lived nuclides $^{168-171}$W. The GSI gas-jet system was used to continuously transport the products attached to KCl particles in 0.83 l/min He carrier gas to the device OlGA II[1]. At the position of the quartz wool plug (oven I) 100 ml/min $Cl_2$ saturated with $SOCl_2$ vapor was added to the carrier gas. Volatile chlorides were transported along the quartz chromatography tube (oven II), ejected into the recluster unit, reattached to new KCl particles (1 l/min $N_2$/KCl) and transported to a glass fibre filter station mounted on top of a HPGe detector. At a fixed temperature setting the gas-jet was switched to OLGA II using a valve, and, after one minute, a single five minute measurement was started for the yield determination. Then, the gas-jet was switched again to the exhaust line and the collecting glass fibre filter was changed for a next measurement at a new temperature setting.

The following $\gamma$-lines were used for detection of W-isotopes: 178.2 keV for $^{168}$W ($T_{1/2} \approx$ 50s); 169.5 keV for $^{169}$W ($T_{1/2} \approx$ 1 min) and 478.7 keV for $^{171A}$W ($T_{1/2} \approx$ 2.5 min).

Figure 1 depicts the measured yields as a function of the temperature of oven II. We observe high yields down to a temperature of about 200 °C which proves the formation of a highly volatile W-chloride species, probably $WOCl_4$ [2].

In Fig. 2 the yield curve is depicted for a fixed temperature of oven II of 300 °C but varying the desorption temperature from the KCl particles. In this case reasonable yields are observed only at temperatures above the melting point of KCl ($T_{m.p.}$ = 760 °C) which seems to indicate that the transported W-atoms are deeply embedded into the KCl agglomerates and, therefore, released only after a major restructuring such as a melting process.

In one experiment a He/$MoO_3$ gas-jet was used. The $MoO_3$ particles were produced in the same way as KCl but at a reduced temperature of the oven of 600 °C.

Fig. 3 depicts the measured yield curve under varying temperatures of the isothermal section of the chromatography column. A slightly higher retention temperature is observed if compared to the measurement with KCl (Fig. 1). This may be caused by the different columns used, which was "filled" in the latter case by a 4 mm thick solid quartz glass rod centered in the middle of the 6 mm i.d. chromatography column. Hence, the chromatographic separation occurred in a 1 mm thick annular slit which should considerably increase the number of theoretical plates in the column.

In the direct catch measurement with $MoO_3$ problems arose with an efficient deposition of the particles on the glass fibre filter. This led to higher than 100 % chemical yields. If, however, the yields were normalized to the KCl direct catch measurements, maximum yields of about 50 % were found, similar to those depicted in Figs. 1 and 2.

As a result, we conclude that W can be easily chlorinated with $Cl_2/SOCl_2$ in OLGA II. Whether a separation of element 106 from elements $\leq$ 105 is possible with such a separation technique can not yet be answered due to lacking studies with Ta, Hf, and the rare earth elements.

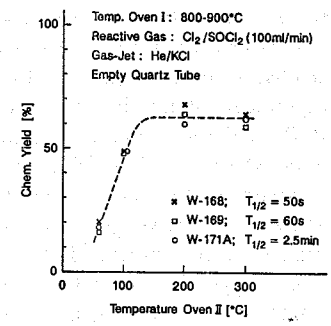


Fig. 1: Yields of tungsten chlorides behind OLGA II as a function of the temperature in the isothermal part of the chromatography column. 100 % represents a direct catch measurement bypassing OLGA II.

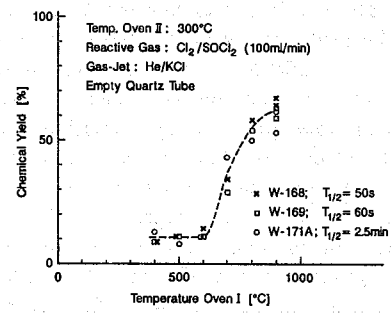


Fig. 2: Same as Fig. 1, but as a function of the desorption temperature from the KCl particles.

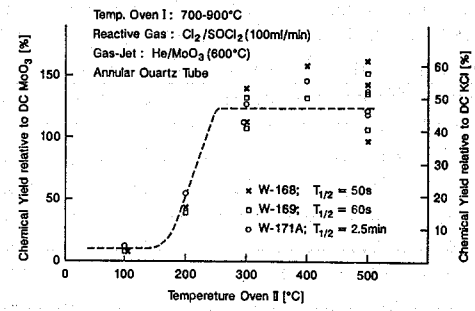


Fig. 3: Same as Fig. 1, but with a He/$MoO_3$ gas-jet system.

[1] H.W. Gäggeler et al., Nucl. Inst. Meth., A309, 201 (1991).
[2] G. Helas et al., Radiochem. Radioanal. Lett., 30, 371 (1977).

# $\alpha$-Particle Measurement from Thin Liquid Films [B]

M.K. Gober[1], H.-U. Becker[1], J.V. Kratz[1], W.J. Krebs[1], U. Tharun[1], N. Trautmann[1], W. Brüchle[2], E. Jäger[2], B. Schausten[2], M. Schädel[2], E. Schimpf[2], H.W. Gäggeler [3], D.T. Jost [3], D. Vermeulen [3]

[1] Institut für Kernchemie der Universität Mainz, [2]GSI Darmstadt, [3]PSI CH-5303 Würenlingen

For further studies of the properties of the heaviest elements fast techniques for chemical separation and sample preparation are required because of the short half-lives of these nuclei far from stability.

With special techniques it is possible to carry out chromatographic separations within a few seconds [1]. The development of large-area passivated ion-implanted planar silicon detectors (PIPS, Canberra/Belgium) gives the opportunity to perform $\alpha$- and spontaneous fission measurements directly from thin liquid films in contact with the detector surface, thus omitting the time consuming preparation of weightless samples for conventional $\alpha$-spectroscopy.

There are certain requirements which must be taken into consideration when constructing such a measuring system: Due to the limited range of $\alpha$-particles and fission fragments in water, the thickness of the liquid film should not exceed some ten $\mu$m to obtain a reasonable energy resolution. Furthermore, the thickness of the liquid layer should be as uniform as possible. Using a 2700 mm$^2$ PIPS detector in a special mount, a counting chamber was constructed. The silicon-detector surface is opposed by a titanium surface at variable distances. The distance is measured by inductive gauge heads with digital readout (TESA, Renens/Switzerland). The resulting volume is sealed by a silicon rubber ring. A 0.3 mm i.d. capillary in the center of the titanium disc serves as inlet. Upon filling the cell, previously introduced liquid is radially removed through twelve 0.3 mm capillaries close to the outer edge. Special precautions have to be taken to make the whole system light tight because the detectors are extremely sensitive to light. The major problem is the achievement of a planar detector surface. The prototype used in 1990 to measure $\alpha$- and sf-decay of element 105 had a very uneven surface which lead to undefined cell volume and layer thickness resulting in a reduced efficiency and poor energy resolution. These problems could be solved by a modified detector mount. This caused a change of the outer dimensions of the detector, so that a new chamber had to be constructed. A schematic drawing is shown in [1]. The chamber can be integrated into the automatic chromatography system ARCA II [2]. It is also possible to pump solution continuously through the chamber with a flow of up to 5 ml/min allowing on-line measurements. Therefore, it may be connected to continuous chromatrographic systems [3] or the SISAK-3 minicentrifuge system [4].

After test measurements with $^{212}$Bi/Po, on-line measurements were performed on 1.8-min $^{226}$Pa produced in the $^{232}$Th(p, 7n)-reaction at the Philips Cyclotron of Paul-Scherrer-Institut, Villigen, Switzerland. The reaction products were transported by means of a He/KCl gas-jet system to a collection frit in ARCA II. The separation by complexation with unbuffered $\alpha$-hydroxyisobutyric acid ($\alpha$-HIB) solution and elution from a strongly acidic cation exchanger was the same as for element 105 and its homologues [1, 5]. The effluent was pumped into the chamber and assayed for $\alpha$-events for 200 s. The thickness of the liquid layer was adjusted to 23 $\mu$m resulting in a calculated volume of 56 $\mu$l which is sufficient to accomodate the $\alpha$-HIB eluate. Fig. 1a shows a spectrum obtained in this cycle. There are several groups of $\alpha$-events which can be attributed to $^{226,227}$Pa and their decay products. To decide wether the surprisingly good energy resolution is due to surface effects, the cell was rinsed carefully several times to remove the activities. The resulting "background" is shown in fig. 1b. This time, one can identify 38-min $^{227}$Pa and 31-min$^{226}$Th and their daughter isotopes. The $\alpha$-activity of $^{226}$Pa is not longer present because of its short halflife. Therefore, one has to draw the conclusion that there is a massive sorption of activities on the detector surface ($SiO_2$). The energy resolution was 175±22 keV FWHM, compared to the roughly 600 keV obtained in the test experiments with $^{212}$Bi/Po. This is another hint that the Pa is sorbed on the detector surface. Further experiments could show wether this effect is limited to the group Vb elements, which show a pronounced tendency for sorption on $SiO_2$ surfaces. This might limit the method to elements with a less problematic behaviour.

[1] M. Schädel et al, GSI-Preprint 92-04 (1992)
[2] M. Schädel et al, Radiochim. Acta 48, 171 (1989)
[3] H. Bruchertseifer et al, Radiochim. Acta 47, 41 (1989)
[4] H. Persson et al, Radiochim. Acta 48, 177 (1989)
[5] H.P. Zimmermann, Doctoral Thesis, Mainz 1992

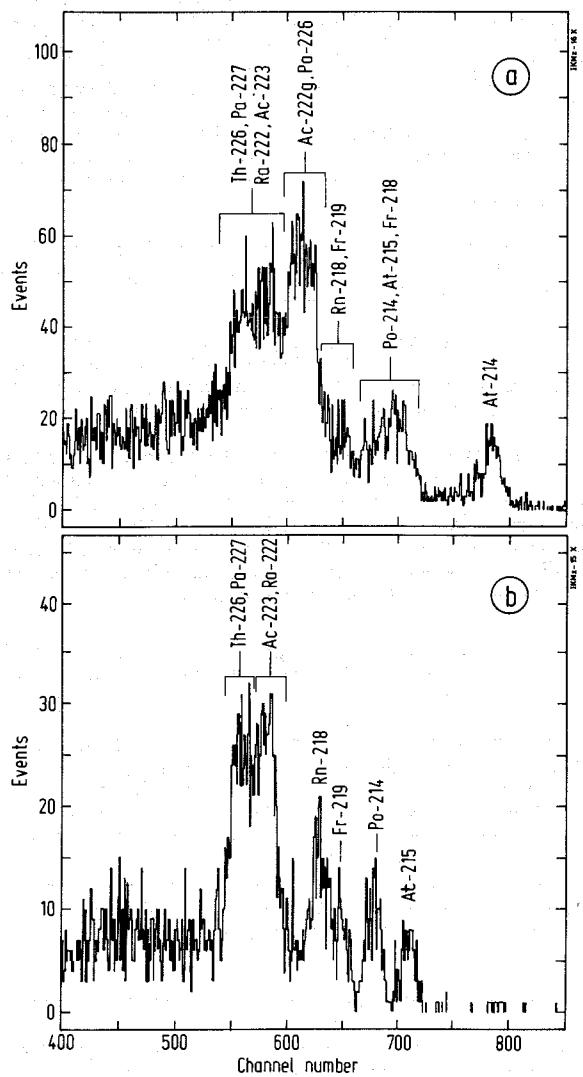


Fig. 1: $\alpha$-spectra of $^{226,227}$Pa and their daughter products measured from a 23 $\mu$m thin liquid film (see text).

# Chemical Transport Reactions of the Element 106 in the $O_2$ - $H_2O$ (g) - System [B]

B.Eichler, S.Hübener
Zentralinstitut für Kernforschung Rossendorf

In addition to halogenating agents a mixture of oxygen and steam could be taken into account as a carrier gas for the characterization of chemical properties of the element 106. Gaschromatographic investigations with the last mentioned gases give the possibility of higher selectivity with regard to other transactinides, actinides or interfering alpha emitters.

The prediction of chemistry of element 106 in $O_2$-$H_2O$ (g) system is necessary to determine the parameters of the gaschemical experiment and to interpret the experimental results. It is expected, that the chemical properties of the element 106 are modified by the influences of the relativistic effects. Experimental data however could only be explained as an influence of the relativistic effect if these results significantly differ from the expections assuming "nonrelativistic" behaviour.

So it is necessary to predict any chemical properties by extrapolation of the properties of the lighter homologous elements in the sixth B-group. The following reactions are particularly important in connection with chemical transport of the element 106:

(1) $MO_3$ (g) ------> $MO_3$ (s)
- desublimation of trioxides;

(2) $(MO_3)_3$ (g) ------> 3 $MO_3$ (g)
- dissociation of trimer trioxides;

(3) M (g) + 4 O (g) + 2 H (g) -> $H_2MO_4$ (g)
- formation of gaseous acid from atoms;

(4) $H_2MO_4$ (g) ------> $MO_3$ (s) + $H_2O$ (g)
- dissociative desublimation of the acid.

Some thermodynamic data [1,2] and results of extrapolations for those processes are compiled in Table 1. The extrapolations were carried out as function of the atomization enthalpies ( $\Delta H^0_{298}$ (g) ) of the metals in the sixth transition group. The value for the element 106 can be estimated to
$\Delta H^0_{298}$ (g) = (900..1156) kJ mol$^{-1}$.
From this limiting values follow the both values for the 106-compounds in Table 1.

The standard entropies of the 106-compounds were estimated by extrapolation from the values for the lighter homologous elements over log(molecular weight). On the base of these thermodynamic functions the gaschemical behaviour in the sequence Cr, Mo, W, 106 can be estimated:
- increasing stability of the trioxides and the acids;
- decreasing volatility of the trioxides;
- increasing tendency to trimerization of the trioxides;
- steam promotes transport reactions;
- the element 106 is probably able to form heteropolynuclear oxides with $MoO_3$ or $WO_3$.

Table 1
Thermodynamic data of the compounds of the sixth group transition metals M in the system M-O2-H2O (g)
( $\Delta H^0$ (kJ mol$^{-1}$) ; $S^0$ (J K$^{-1}$ mol$^{-1}$) ; standard states)

| M | $\Delta H^0$f MO3 (s) | $\Delta H^0$f MO3 (g) | $\Delta H^0$desub MO3 reaction (1) |
|---|---|---|---|
| Cr | - 589 | -272 | -317 |
| Mo | - 745 | -346 | -399 |
| W | - 843 | -293 | -550 |
| 106 | - 873 | -346 | -527 |
| | -1016 | -390 | -626 |

| M | $\Delta H^0$diss (MO3)3 (g) reaction (2) | $\Delta H^*$f H2MO4 (g) reaction (3) | $\Delta H^0$diss.des. H2MO4 (g) reaction (4) |
|---|---|---|---|
| Cr | 749 | -2586 | - 95 |
| Mo | 836 | -2945 | -138 |
| W | 1126 | -3127 | -177 |
| 106 | - | -3245 | -185 |
| | | -3614 | -267 |

| compound | $S^0$ (s) | $S^0$ (g) | $\Delta S^0$desubl |
|---|---|---|---|
| (106)O2 | 51 | 290 | -239 |
| (106)O3 | 88 | 300 | -212 |
| H2(106)O4 | 130 | 352 | -222 |

The formation of mixed polymer oxides may be used as a test for the similarity with Mo as well as with W . It is possible that weighable amounts of $MoO_3$ or $WO_3$ modify the transport reactions of the element 106. The presented data permit an estimation of the adsorption behaviour of the 106 compounds at the quartz surface - a necessary condition for planning of gaschemical experiments with the element 106 in its oxide or hydroxide forms.

References

[1] J.Phys.Chem. Ref. Data 14, Suppl. 1 (1985).
[2] Dellien J. , Chemical Reviews 76 ,283 (1976).

# On-line isothermal gas chemistry experiments with protactinium chloride

D.T. Jost, U. Baltensperger, U. Bochert, H.W. Gäggeler, A. Kovacs, A. Weber
Paul Scherrer Institut, Villigen Switzerland

B. Eichler
ZfK-Rossendorf

H. Bruchertseifer, W. Heller
ZfI Leipzig

U. Becker, M. Gober, J.V. Kratz
Universität Mainz

M. Schädel
GSI-Darmstadt

G. Pfepper, S.N. Timokhin
JINR-Dubna

In the course of the studies on the chemical properties of element 105, a transition element of group 5, interest came up to also investigate the chemical properties of Pa, a pseudo-group 5 element.

We have produced $^{226}$Pa ($T_{1/2}$ = 1.8 min) and $^{227}$Pa ($T_{1/2}$ = 38.3 min) in a bombardment of a stack containing 15 50 µg/cm$^2$ thick $^{232}$Th targets[1] with a 58 MeV p beam. The energy loss in the targets was 5 MeV and the beam intensity about 300 nA.

Products were transported with a 2 l/min He/KCl gas-jet through a about 100 m long 2 mm i.d. polyethylene capillary to the gas chemistry apparatus OLGA II[2].

As reactive gas 100 ml $Cl_2$ saturated with $SOCl_2$ vapor was added at the position of the quartz wool plug. Behind the reclustering unit of OLGA II (1 l/min $N_2$/KCl) the products were transported to the tape counting system. The stepping time was one minute and the activity was measured in counting chamber # 1 with a 300 mm$^2$ PIPS detector. No detectors were mounted in the counting chambers # 2 to 6 (for details see ref. 2). Only $^{226}$Pa was analyzed.

Figure 1 shows the relative chemical yields for $^{226}$Pa as a function of the temperature of the isothermal part (oven II) of the quartz chromatography column. Maximum yields are observed for temperatures > 750 °C, which indicates either a low volatility of the separated species or a strong interaction with the column surface (presumably KCl).

In one experiment a He/$MoO_3$ gas-jet was used. Surprisingly, with $MoO_3$ particles (produced at 600 °C) a "more volatile" Pa chloride species was observed (Fig. 2). It is well known that Mo forms very volatile oxy-chlorides which means that in this case the chromatography column is not covered with $MoO_3$.

In Table 1 deposition temperatures of Pa - chloride molecules from thermochromatography experiments are summarized. These experiments were performed in glass columns. Also listed in Table 1 are our "50 % - chemical yield" temperatures, which should be roughly equal to the deposition temperatures from thermochromatography experiments[3].

Obviously, the value from the KCl gas-jet experiment disagrees remarkably from all other data which seems to indicate a strong interaction of the Pa - chloride molecules in the chromatography column with the KCl surface.

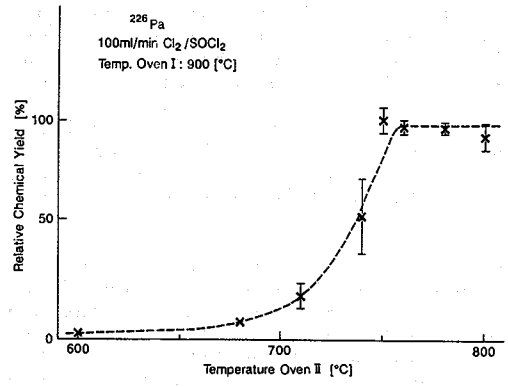


Fig. 1: Yield curve for $^{226}$Pa-chloride molecules with a He/KCl gas-jet and $Cl_2/SOCl_2$ as chlorinating agent.

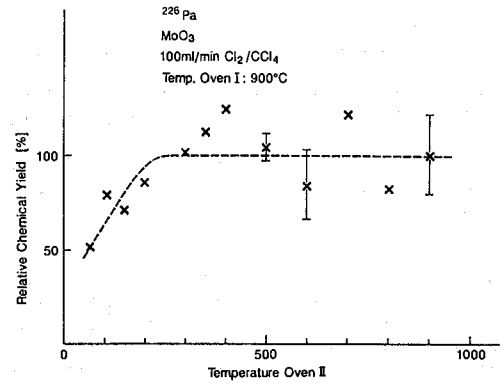


Fig. 2: Same as Fig. 1 but with a He/$MoO_3$ gas-jet and $Cl_2/CCl_4$ as chlorinating agent.

Table 1: Gas chemistry data of Pa - chlorides

| Nuclide | Temperature [°C] | Reactive gas | Ref. |
|---|---|---|---|
| $^{233}$Pa | 95 (TC) | $CCl_4 + Cl_2$ | 4 |
| $^{?}$Pa | 300 (TC) | $SOCl_2$ | 5 |
| $^{226}$Pa | 90 (IC/$MoO_3$) | $CCl_4 + Cl_2$ | Th. work |
| $^{226}$Pa | 740 (IC/KCl) | $SOCl_2 + Cl_2$ | Th. work |

TC: Deposition temp. from thermochromatography experiment

IC: "50 % - chemical yield" temperature

[1] A. Kovacs et al., Annual Report 1991, Paul Scherrer Institut, Division F3A (1992).
[2] H.W. Gäggeler et al., Nucl. Inst. Meth., A309, 201 (1991).
[3] H.W. Gäggeler et al., PSI-PR-91-32, and submitted to Radiochim. Acta (1991)
[4] J. Merinis et al., Radiochem. Radioanal. Lett., *3*, 255(1970)
[5] T.S. Zvarova et al., Report JINR, P6-4130, Dubna (1968)

# Thermodynamical Volatility of Element 105 Halides[G]

V. Pershina, B. Fricke
Physics Department, University of Kassel
G. Ionova
Institute of Physical Chemistry, USSR Academy of Sciences, Moscow
M. Schädel
GSI Darmstadt

In macrochemistry volatility is determined through the Maxwell equation, connecting volatility, volume, temperature and entropy of a substance

$$\left(\frac{\partial P}{\partial T}\right)_V = \left(\frac{\partial S}{\partial V}\right)_T , \quad \frac{dP}{dT} = \frac{\Delta S_T}{\Delta V_T} . \qquad (1)$$

In reality the temperature dependence of the vapour pressure is used to get information about volatility of a substance. From chemical experiments these dependences for $NbBr_5$ and $TaBr_5$ are

$$\log P_{mm} = 12.5 - \frac{5782}{T} \qquad (205 - 252°C) \qquad (2)$$

$$\log P_{mm} = 12.5 - \frac{5546}{T} \qquad (180 - 255°C) \qquad (3)$$

In the temperature interval between 180 and 320 °C the vapour pressure of $TaBr_5$ is a factor of 1,5 - 2 higher that of $NbBr_5$.

In the area of low temperatures and low pressure

$$\log \frac{P_{NbBr_5}}{P_{TaBr_5}} = -\frac{B_{TaBr_5}(1-\gamma)}{T} , \quad \gamma = \frac{B_{NbBr_5}}{B_{TaBr_5}} . \qquad (4)$$

If to assume that $\gamma$ is determined by attraction energy between two identical molecules (e.g. $NbBr_5$ and $NbBr_5$) and that the two $MBr_5$ molecules interact via the two adjacent bromine atoms, $\gamma$ could be expressed through the dispersion interaction energy $\varepsilon(x)$ of the bromine atoms in these molecules:

$$\gamma = \frac{\varepsilon(x)_{NbBr_5}}{\varepsilon(x)_{TaBr_5}} = \frac{I_{Br}^{NbBr_5}(\alpha_{Br}^2)^{NbBr_5}}{I_{Br}^{TaBr_5}(\alpha_{Br}^2)^{TaBr_5}} , \qquad (5)$$

where $I_{Br}$ is ionization potential and $\alpha_{Br}$ is polarizability of the bromine atom in a molecule.

Taking into account that polarizability of a spherically symmetric atom is expressed as a cube of mean radius $<r>$ of its electron shell we have

$$\gamma = \frac{I_{Br}^{NbBr_5}(r_{Br}^6)^{NbBr_5}}{I_{Br}^{TaBr_5}(r_{Br}^6)^{TaBr_5}} , \qquad (6)$$

where dependences of $r$ and $I$ on effective charge Q on the bromine atom are

$$r_{Br}(Q) = 1.14 - 0.85Q \qquad (Q < 0)$$

and

$$I_{Br}(Q) = 273 + 194Q \ (kcal) . \qquad (Q < 0)$$

For the relation (6) experiments give $\gamma$ = 1.04. Using the values of effective charges $Q_{Br}$ from our molecular orbital calculations[1] we find for the hahnium pentabromide

$$\gamma = \log \frac{P_{TaBr_5}}{P_{HaBr_5}} = 1.09.$$

Thus $HaBr_5$ molecules should have weaker disperse interaction and higher vapour pressure compared to $TaBr_5$ at any fixed temperature. Assuming that within the temperature range between 200 and 250 °C $\log P_{HaBr_5}$ has a form similar to Eqs. (2,3), the dependence of log P on T can be expressed as

$$\log P_{HaBr_5} = 12.5 - \frac{5088}{T} . \qquad (7)$$

The plot $P_{mm}$(Hg) vs. T [Eq. (7)] for $HaBr_5$ is shown on Fig. 1.

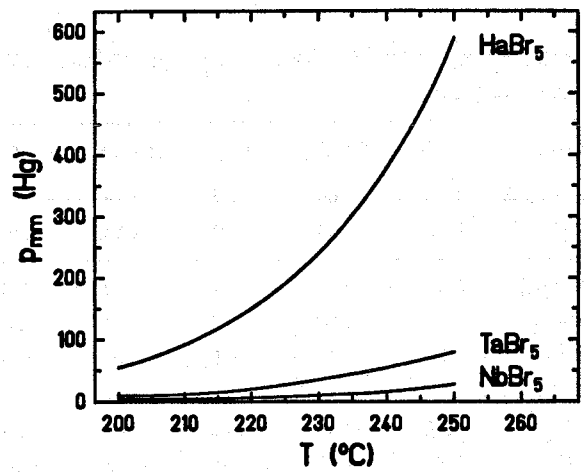


Fig.1: Volatility of $MBr_5$, where M = Nb, Ta and Ha, within the temperature interval 200 - 250 °C.

1. Pershina V. G., Sepp W.-D., Fricke B., et al, to be published (1991)

# Electronic Structure of Hahnium Oxyhalides as Analogs of Group 5 Element Oxyhalides[G]

V. Pershina, W.-D. Sepp, B. Fricke, T. Bastug
Physics Department, University of Kassel

Gas phase experiments[1] on studying volatility of halides of element 105, hahnium, along with its analogs gave impact to relativistic calculations of their electronic structure[2]. Estimations of the volatility on the basis of these calculations have shown that hahnium compounds should be more volatile than the compounds of niobium, tantalum and protactinium. In the macro chemistry formation of the pure halides ($MCl_5$ or $MBr_5$) is often accompanied by formation of the oxyhalides ($MOCl_3$ or $MOBr_3$). In the presence of traces of oxygen at 150 ÷ 200 °C pure pentahalides transform into the oxyhalide forms. Thus a natural continuation of the work[1] was investigation of the electronic structure and properties of the oxytrihalides of these elements.

Relativistic molecular orbital calculations of $MOCl_3$ and $MOBr_3$ species, where M = V, Nb, Ta, Pa and Ha, have been done using relativistic Dirac-Slater Discrete-Variational method.

According to the gas-phase Raman spectra of $VOCl_3$ and $NbOCl_3$ the oxyhalides of Ta, Ha and Pa are supposed to be monomers possessing $C_{3v}$ symmetry. The energy level diagrams as a result of the calculations are shown in Fig. 1. Table 1 contains the brief summary of the results (for $MOBr_3$ molecules all the trends within the group are the same).

Table 1

Overlap populations (n), effective atomic charges (Q) and dipole moments for $MOCl_3$

| Molecule | $VOCl_3$ | $NbOCl_3$ | $TaOCl_3$ | $HaOCl_3$ | $PaOCL_3$ |
|---|---|---|---|---|---|
| R(M=O), Å | 1.56 | 1.66 | 1.66 | 1.74 | 1.70 |
| R(M-Cl), Å | 2.12 | 2.24 | 2.25 | 2.33 | 2.52 |
| n(M=O) | 0.59 | 0.63 | 0.72 | 0.79 | 0.42 |
| n(M-Cl) | 1.21 | 1.13 | 1.44 | 1.50 | 1.19 |
| n(tot) | 1.80 | 1.76 | 2.16 | 2.29 | 1.62 |
| $Q_M$ | 1.17 | 0.98 | 1.02 | 0.89 | 1.14 |
| $Q_O$ | -0.40 | -0.37 | -0.40 | -0.40 | -0.39 |
| $Q_{Cl}$ | -0.26 | -0.20 | -0.21 | -0.17 | -0.25 |
| $\mu$, D | 0.48 | 0.91 | 0.99 | 1.27 | 0.88 |

Here overlap population (n) is the amount of electron density between atoms and it is a measure of covalent bonding.

One can see that the electronic structure of $HaOCl_3$ is similar to those of Nb and Ta. The tendency of the metals to form double bonds with oxygen increases in going from V to Ha. The total overlap population also increases in this direction indicating that the hahnium compounds are the most covalent ones. Effective charges on the atoms show decreasing ionicity in going from V to Ha. $PaOCl_3$ has quite a different electronic structure with much lower covalency (and hence lower bonding) and smaller metal-oxygen overlap.

In contrast with expectations the results have shown that MOCl compounds are more ionic than the corresponding MCl ones. The lower covalency of the $MOCl_3$ species gives partially an explanation of their lower volatility compared to that of the pure pentachlorides. Besides the lower covalency the dipole-dipole interaction of $MOCl_3$ molecules also contributes to their lower volatility. Supposing that $HaOCl_3$ has the same dimer structure in the solid state as $NbOCl_3$ and $TaOCl_3$, its higher covalency compared to them is indicative of its higher volatilty. $PaOCl_3$ being more ionic molecule should have the lowest volatility.

Some preliminary qualitative estimations of the volatility of the oxibromides (in case they are formed during the bromination of the metal in the gas phase experiments[1]) could be made on the basis of the molecular-orbital calculations. Thus $HaOBr_3$ should be obviously more volatile than $NbOBr_3$, $TaOBr_3$ and $PaOBr_3$ due to the lower effective charges and as a consequence - the lower Coulomb interaction with the ionic surface. The same is valid for the $MOCl_3$ and $MCl_5$ molecules. But only presise calculations of the adsorption process could give a quantitative answer.

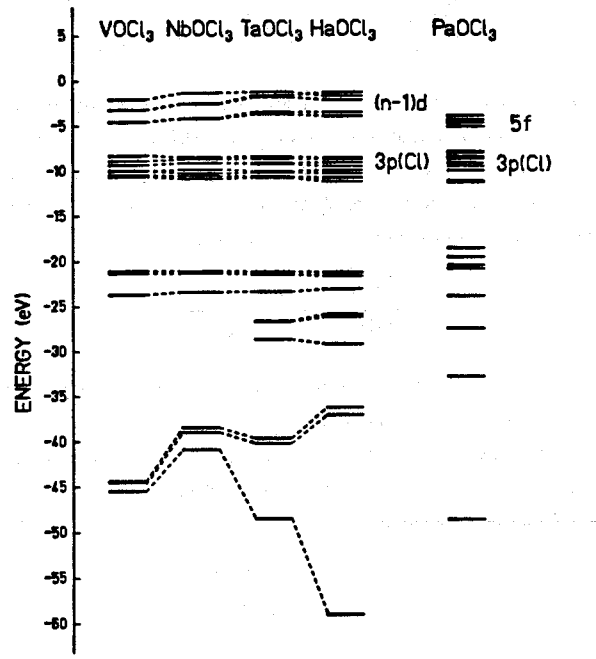


Fig.1: Energy eigenvalues of the outer electrons for $MOCl_3$

1. Gäggeler H.W., Jost D.T., Kovacs J. et al., PSI Bericht, PSI - PR -91-32 (1991)
2. Pershina V. G., Sepp W.-D., Fricke B., GSI Scientific Report 1990, GSI 91-1 (1991), p. 275., submitted to J. Chem. Phys.

# Standard Oxidation Potentials $E^0(M^{z+}/M^{z'+})$ for Group 5 Elements[G]

G. Ionova

Institute of Physical Chemistry, USSR Academy of Sciences, Moscow

V. Pershina, B. Fricke

Physics Department, University of Kassel

The chemistry of niubium and tantalum ranges from oxidation states +5 to -3, but with no species of oxidation state -2 presently known. The small difference between energy levels of d- and s-electrons gives rise to a wide range of oxidation states. For the characteristic of oxidation state the oxidation-reduction potential $E^0$ is of crucial importance. The complete picture of the reduction-oxidation properties of the group 5 elements must include potentials $M \rightarrow M^{5+}$, $M^{5+} \rightarrow M^{4+}$, $M^{4+} \rightarrow M^{3+}$, $M^{3+} \rightarrow M^{2+}$, $M^{2+} \rightarrow M^{1+}$.

The free energy $\Delta F$ of the reaction $M^{z+n} + ne = M^z$ should be written as

$$\Delta F = -23060En \qquad (cal) \ . \tag{1}$$

For $M^{5+} + 5e \rightarrow M$ we can write the reaction

$$M_2O_5 + 10H^+ + 10e \rightarrow 2M + 5H_2O \ . \tag{2}$$

The free energy $\Delta F^0$ of the reaction (2) is

$$\Delta F^0 = 2F^0_M + 5F^0_{H_2O} - F^0_{M_2O_5} - 10F^0_{H^+}. \tag{3}$$

Then $E^0(M^{5+}/M)$ is defined as

$$E^0 = \frac{5(-56690) + F^0_{M_2O_5}}{10 \cdot 23060} \ . \tag{4}$$

From correlation $E^0(M^{5+}/M)$ with the sum of ionization potentials $\sum_{i=0}^{5} I_i$ for group 5 elements[1] we obtain $E^0(Ha^{5+}/Ha) = -0.83$ V (Fig. 1). So $E^0(Ha^{5+}/Ha)$ is between $E^0(M^{5+}/M)$ for Ta and Pa. Using this value of $E^0$ the free formation energy for $Ha_2O_5$ is -474.85 kcal.

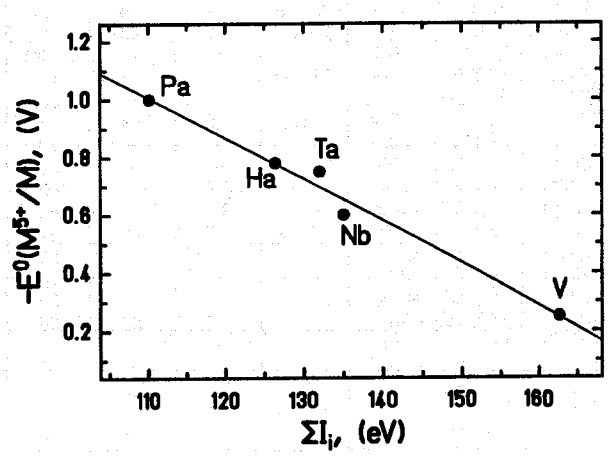


Fig.1: Correlation between the sum of ionization potentials $\sum_{i=0}^{5} I_i$ and reduction potentials $E^0(M^{5+}/M)$ for group 5 elements.

For reaction $M^{5+} \rightarrow M^{4+}$ only two redox potentials $E^0(M^{5+}/M^{4+})$ have been measured: for V and Pa. Correlation of the redox potentials with the fifth ionization potentials results in the values $E^0(M^{5+}/M^{4+})$ for Nb, Ta and Ha listed in Table 1. This means that the stability of the tetravalent state in solution decreases from V to Ha:

$$V \gg Nb > Ta > Pa > Ha.$$

So in solutions the oxovanadium ion (4+) in the presence of a strong acid is stable for months and $Ha^{4+}$ is less stable in comparison with $Pa^{4+}$.

For reaction $M^{4+} \rightarrow M^{3+}$ we can estimate $E^0(Nb^{4+}/Nb^{3+})$ using known value of $E^0(Nb^{5+}/Nb^{3+}) \simeq -0.1$ V and evaluated by us $E^0(Nb^{5+}/Nb^{4+}) = 0.14$ V using equation

$$E^0(Nb^{5+}/Nb^{3+}) = 1/2[E^0(Nb^{5+}/Nb^{4+}) + E^0(Nb^{4+}/Nb^{3+})].$$

Correlation of the fourth ionization potentials[1] with the $E^0(M^{4+}/M^{3+})$ for V, Nb and Pa results in the values for Ta and Ha given in Table 1. So stability of the trivalent state in aqueous solutions is the smallest for Pa, and $Ha^{3+}$ is more stable than $Pa^{3+}$.

There are nearly no $E^0$ data for the reaction $M^{3+} + e \rightarrow M^{2+}$. A very crude evaluation of $E^0(M^{4+}/M^{3+})$ for Nb, Ta and Ha can be made using $E^0(M^{4+}/M^{3+})$ for V and Pa, and correlation between the $E^0(M^{4+}/M^{3+})$ and the third ionization potentials[1].

More accurately evaluation of the potentials $E^0(M^{3+}/M)$ can be done using the thermodynamic formula

$$E^0(M^{3+}/M) = \frac{5E^0(M^{5+}/M) - E^0(M^{4+}/M^{3+}) - E^0(M^{5+}/M^{4+})}{3} \ .$$

Table 1

Redox potentials for V, Nb, Ta, Ha, and Pa

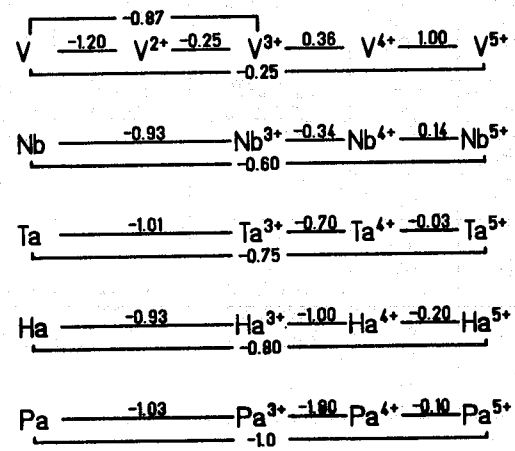


There is possibility for Nb to exist in the mixed-valence complexes in solutions. This could be valid also for Ha since Nb and Ha have close to each other values of potentials $E^0(M^{3+}/M^{2+})$.

1. Johnson E. and Fricke B., to be published (1991)